CDF/TOP/DOC/CDFR/9417
Draft 0.1
November 20, 2008

Search for Pair Production of Stop Quarks Mimicking Top Event Signatures

Andrew Ivanov[1], Will Johnson[2],
Robin Erbacher[3]

University of California, Davis

Abstract

We update the search for the pair-produced super-symmetric partner of the top quark (stop quark) from $1.9fb^{-1}$ to $2.7fb^{-1}$ of data collected with CDF II. We search for the scalar top quarks via their decay channel: $\tilde{t}_1 \to b\tilde{\chi}_1^{\pm} \to b\tilde{\chi}_1^0 l\nu$, which gives an event signature similar to that of a top dilepton event. We reconstruct events under the stop decay hypothesis and use the reconstructed stop mass as a discriminative kinematic variable in the fit.

In the signal region the number of events observed is in agreement with the number expected from the SM processes. The kinematic distribution of the stop reconstructed mass is also consistent with the SM predictions. Thus no evidence for scalar top quark pair-production is observed. We place a limit on the dilepton branching ratio of stop quarks in a three-dimensional space of masses of super-symmetric particles $\tilde{t}_1, \tilde{\chi}_1^{\pm}, \tilde{\chi}_1^0$.

Contents

[1]andrew@fnal.gov
[2]wcjohnson@physics.ucdavis.edu
[3]erbacher@physics.ucdavis.edu

1 Introduction

We update our previous search (cdf note 9269 [6]) from $1.9 fb^{-1}$ to $2.7 fb^{-1}$, employing the same limit setting procedures, and using similar prescriptions to compute systematics.

We search for the pair-produced supersymetric partner of the top quarks, the stop quark, at masses similar to the SM top quark and below. We consider stop quark decays giving a final state event signature similar to that of top dilepton events, but different from top events by the addition of 2 massive undetected neutralinoes. We look for events with two leptons, two b-jets and large $\not\!\!E_T$.

Since the stop quark is a scalar particle the production cross section at the Tevatron is about an order of magnitude lower than for a fermionic quark with a similar mass, which in addition to the relatively large top quark dominated background, makes this a challenging search.

To discriminate stop events from the SM background, we perform a weighted reconstruction of candidate events under the stop hypothesis, and use the reconstructed stop mass as a discriminating variable between stop, and the SM, utilizing both rate and shape information, separately for the b-tagged and untagged channels.

For detailed experimental and theoretical motivations of this search, as well as additional analysis details see [6].

1.1 Stop Quark Production at the Tevatron

At the Tevatron the stop quarks would be produced in pairs via the QCD processes shown in in Figure 1. The stop quark pair production cross section depends on the stop quark mass, and is independent of other SUSY parameters. The NLO production cross sections for various stop masses are listed in Table 1. They were obtained using PROSPINO 2.0 [2] and CTEQ6M (NLO) parton distribution functions.

$m_{\tilde{t}_1}$, GeV	$\sigma_{NLO}(\tilde{t}_1\bar{\tilde{t}}_1)$, pb
115.0	6.89
135.0	2.77
155.0	1.23
185.0	0.416

Table 1: Cross section in pb for $\tilde{t}\bar{\tilde{t}}$ production at the Tevatron.

1.2 Scalar Top Quark Decays

The decays of the stop quarks are dictated by the mass spectrum of other supersymmetric particles. For a light stop, $m_{\tilde{t}_1} \lesssim m_t$, and the R-parity conserved SUSY the

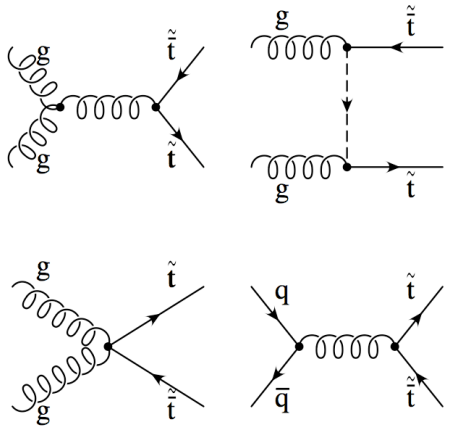

Figure 1: The dominant processes for stop quark pair production at the Tevatron.

following decays are possible:

$$\tilde{t}_1 \to c\tilde{\chi}^0_{1,2}, \quad \tilde{t}_1 \to b\,\chi^+_1, \quad \tilde{t}_1 \to W^+\,b\,\tilde{\chi}^0_1, \quad \tilde{t}_1 \to H^+\,b\,\tilde{\chi}^0_1, \quad \tilde{t}_1 \to b\,\tilde{\ell}^+\,\nu_\ell, \quad \tilde{t}_1 \to b\,\tilde{\nu}_\ell\,\ell^+$$

For reasons that will be discussed shortly we choose to investigate

$$\tilde{t}_1 \to b\,\chi^+_1 \tag{1}$$

and consider the cases where the $\tilde{\chi}^\pm_1$ can decay to our desired dilepton final state via

$$\tilde{\chi}^\pm_1 \to \tilde{\chi}^0_1 + W^{\pm(*)} \to \tilde{\chi}^0_1 + \ell + \nu \quad (2) \qquad \tilde{\chi}^\pm_1 \to \tilde{\chi}^0_1 + H^{\pm *} \to \tilde{\chi}^0_1 + \ell + \nu \quad (3)$$

$$\tilde{\chi}^\pm_1 \to \ell + \tilde{\nu}_\ell \to \tilde{\chi}^0_1 + \ell + \nu \quad (4) \qquad \tilde{\chi}^\pm_1 \to \nu + \tilde{\ell}_L \to \tilde{\chi}^0_1 + \ell + \nu \quad (5)$$

$$\tilde{\chi}^\pm_1 \to \tilde{\chi}^0_1 + G^{\pm *} \to \tilde{\chi}^0_1 + \ell + \nu \quad (6)$$

Where if $m_{\tilde{\chi}^\pm_1} - m_{\tilde{\chi}^0_1} \geq m_{W^\pm}$ then (2) will dominate over the other possible decay means. If the charginos decay through (2), then the dilepton branching ratio of stop events will be the same as top events, 0.11. However, when the other chargino decay modes are possible, the dilepton branching ratios will become dependent on other SUSY parameters, and can possible greatly enhance the dilepton branching ratio. For instance, at $m_{\tilde{\chi}^\pm_1} = 105.8$ and $m_{\tilde{\chi}^0_1} = 58.8$ GeV, the stop events have a dilepton branching ratio of 0.25 at $tan\beta = 5$, but at $tan\beta = 15$ the dilepton branching ratio increases to 0.50.

2 Methodology

2.1 Goals

What distinguishes this search from most of other SUSY searches is that one can obtain results independent of the complex multi-variate phase space of SUSY parameters. The minimal assumptions made here are:

1. $\tilde{\chi}_1^0$ is the LSP, and $\tilde{q}, \tilde{\ell}, \tilde{\nu}$ are heavy
2. $m_{\tilde{t}_1} \lesssim m_t$
3. $m_{\tilde{\chi}_1^+} < m_{\tilde{t}_1} - m_b$

If these requirements are satisfied the channel (1) has 100% branching ratio. The rate with which the $\tilde{t}_1\bar{\tilde{t}}_1$ events are produced depend on $m_{\tilde{t}_1}$, and kinematics of the stop events depend on masses of super-symmetric particles: ($m_{\tilde{t}_1}$, $m_{\tilde{\chi}_1^+}$, $m_{\chi_1^0}$)

Therefore in this analysis we aim to explore the three-dimensional phase space of masses of these super-symmetric particles, and in the absence of new physics evidence we can derive limits on masses of $\tilde{t}_1, \tilde{\chi}_1^\pm, \tilde{\chi}_1^0$ independent on other SUSY assumptions.

2.2 Means

For the first version of the analysis, the event selection cuts were optimized to maximize expected exclusion sensitivity, taking into account nearly all systematic uncertainties. All event selection cuts, and prescription for computing systematic uncertainties remain identical to the $1.9 fb^{-1}$ search. We have updated all scale factors and uncertainties to reflect the new data, and recomputed all systematic uncertainties.

We employ the CL_s likelihood fit technique, described in Ref. [30], that embeds all of the systematic parameters into the fit and allows morphing the kinematic distribution shape as a function of those parameters.

3 Data Sample and Dilepton Selection

3.1 Datasets and Luminosity

This analysis is based on the data collected by CDF II through data period 17, using inclusive high-P_T lepton triggers listed in Table 2. We use CDF Silicon Good Run List, version 23 [15] with runs 222414 and 222418 excluded due to MC and beam line position problems, and for runs 230536, 231179, 231241, 231334, 236653, 235056, 236040 use only first 1,800 run segments due to missing beam line.

Dataset names used in this analysis and their corresponding luminosities are listed in Table 3. The total integrated luminosity of the analyzed data is 2.7 fb^{-1}. The total luminosity for CMX triggers is a bit smaller than for CEM and CMUP due to exclusion of runs prior to 150145 (no triggering on CMX possible), and due to use of dynamically pre-scaled (DPS) triggers for the later periods of data.

3.2 Lepton Identification and Dilepton Selection

We select the lepton types following the CDF's Joint Physics selection criteria [16, 17]. One of the leptons is required to be a tight central lepton (CEM, CMUP or CMX), while the second lepton can satisfy looser requirements. Specifically, the second lepton can be one of the following: non-isolated central electron (NICEM), forward electron (PHX), CMU or CMP-only muon, non-isolated muon (NICMUP, NICMX, NICMU, NICMP) or a minimum-ionizing particle (CMIO). Various dilepton categories are constructed from the combination of tight-tight and tight-loose lepton pairs. Although the PHX electron

Trigger Path	**Run Range**
ELECTRON_CENTRAL_18	138425 - 261005
MUON_CMUP18	138425 - 229763
MUON_CMUP18_L2_PT15	229763 - 261005
MUON_CMX18	150145 - 200272
MUON_CMX18_L2_PT15	150145 - 226194
MUON_CMX18_L2_PT15_LUMI_200	200273 - 226194
MUON_CMX18_&_JET10	226195 - 257201
MUON_CMX18_&_JET10_LUMI_270	226195 - 257201
MUON_CMX18_&_JET10_DPS	226195 - 257201
MUON_CMX18	$\geq$ 257201

Table 2: Trigger paths used in this analysis and corresponding run ranges [13].

Period	**Run Range**	**Dataset Name**	**Luminosity (pb^{-1})**	
			CEM/CMUP	CMX
0	138425-186598	bhel(mu)0d	331.47	318.11
1-4	190697-203799	bhel(mu)0h	362.94	359.50
5-7	203819-212133	bhel(mu)0i	258.37	258.37
8	217990-222426	bhel(mu)0i	166.29	166.29
9	222529-228596	bhel(mu)0i	156.76	152.78
10	228644-233111	bhel(mu)0i	243.19	243.49
11	233133 - 237795	bhel(mu)0j	234.99	229.98
12	237845 - 241664	bhel(mu)0j	162.01	155.25
13	241665 - 246231	bhel(mu)0j	280.86	268.35
14	252836 - 254686	bhel(mu)0k	32.01	30.59
15	254800 - 256824	bhel(mu)0k	161.87	156.36
16	256840 - 258787	bhel(mu)0k	101.81	100.74
17	258880 - 261005	bhel(mu)0k	183.56	182.93
Total			2676.13	2622.74

Table 3: Datasets used in this analysis and corresponding luminosities [14].

falls into the second category, the combinations: PHX - NI(CEM, CMUP, CMX) are also allowed. This dilepton selection is similar to the top dilepton analysis [18] with an exception that CMIOs are required to be fiducial to CEM towers of the detector (fidEle = 1). We place this requirement to remove electrons going through the edges of calorimeter towers, depositing a small energy in the calorimeter and thus faking CMIO, We found the rate of this happening in data vs MC was significantly different.

Lepton identification criteria are listed in Tables 4 and 5.

3.3 Lepton Trigger Efficiencies and Scale Factors

We take into account lepton trigger efficiencies and differences in reconstruction efficiencies between data and Monte Carlo using corresponding scale factors obtained from the Joint Physics web-page and applied using the Joint Physics Scale Factor Class [19]. These tools are not directly applicable for dilepton categories, however, because any of a pair of leptons could trigger an event. Therefore, we construct the scale factor per each dilepton category, as follows

$$C_{\ell_1\ell_2} = \epsilon_{z_0} \times (\epsilon_{trig1} + \epsilon_{trig2}\epsilon_{dps2} - \epsilon_{trig1}\epsilon_{trig2}\epsilon_{dps2}) \times SF_1 SF_2, \tag{7}$$

where ϵ_{z_0} is the efficiency of the event vertex $|z_0| < 60$ cm cut, ϵ_{trig1} and ϵ_{trig2} are trigger efficiencies of the first and the second lepton, and $SF_i = \epsilon^{data}_{reco,i}/\epsilon^{MC}_{reco,i}$ are their reconstruction scale factors. We assume that a non-isolated lepton has the same efficiency as its isolated analog, i.e. for instance, $\epsilon_{trig,CEM} \equiv \epsilon_{trig,NICEM}$ while efficiencies for non-trigger leptons ((NI)CMU, (NI)CMP, PHX and CMIO) are identically zero. The dilepton scale factor (7) is unique per each data period, when there are no DPS triggers. For the periods where the CMX trigger was dynamically pre-scaled the DPS trigger efficiency ϵ_{dps} is computed per each run section based on the pre-scale value of the trigger for a given period of time.

(NI)CEM	PHX
$E_T \geq 20$ GeV	$E_T \geq 20$ GeV
E/p ≤ 2 (unless $p_T \geq 50$ GeV/c)	
$E_{had}/E_{em} \leq 0.055 + 0.00045E$	$E_{had}/E_{em} \leq 0.05$
$L_{shr} \leq 0.2$	$\chi^2_{PEM} \leq 10$
Track $p_T \geq 10$ GeV/c	Phoenix Track
Track $\|z_0\| \leq 60$ cm	Phoenix $\|z_0\| \leq 60$ cm
Ax SLs with 5 hits/SL ≥ 3	Si Hits ≥ 3
St SLs with 5 hits/SL ≥ 2	
Fiducial to CES	$1.2 \leq \|\eta_{PES\_2D}\| \leq 2.8$
$\|\Delta z_{CES}\| < 3$ cm	PES 5×9 U ≥ 0.65
-3 cm $\leq Q \times \Delta x_{CES} \leq 1.5$ cm	PES 5×9 U ≥ 0.65
$\chi^2_{CES} \leq 10$	$\Delta R_{PES,PEM} \leq 3$ cm
Photon Conversion Veto	
Iso($\Delta R = 0.4/E_T$) ≤ 0.1 (unless NI)	Iso($\Delta R = 0.4/E_T$) ≤ 0.1

Table 4: Electron Identification Criteria

(NI) (CMUP / CMU / CMP)	(NI)CMX	CMIO
$p_T \geq 20$ GeV/c		
Ax SLs with 5 hits/SL ≥ 3		
St SLs with 5 hits/SL ≥ 2		
Track $\|z_0\| \leq 60$ cm		
$d_0 <$ (w/Si Hits 0.02, w/o 0.2) cm		
$E_{em} <$ 2 GeV + max(0,0.0115*(p-100))		
$E_{had} <$ 6 GeV + max(0,0.028*(p-100))		
Iso($\Delta R = 0.4/E_T$) ≤ 0.1 (unless NI)		
$\|\Delta x_{CMU}\| < 7$ cm (for CMUP,CMU)	$\|\Delta x_{CMX}\| < 6$ cm	$E_{em} + E_{had} \geq 0.1$
$\|\Delta x_{CMP}\| < 5$ cm (for CMUP,CMP)	$\rho_{COT} > 140$ cm	Fiducial to CES
Fiducial $x_{CMUP,CMU,CMP} < 0$ cm	Fiducial $x_{CMX} < 0$ cm	Non-fudical
Fiducial $z_{CMUP,CMU} < -3$ cm	Fiducial $z_{CMX} < -3$ cm	Non-fudical
Fiducial $z_{CMP} < 0$ cm		Non-fiducial

Table 5: Muon Identification Criteria

4 Event Selection

Event selection for this analysis was optimized based on expected exclusion for the 1.9 fb^{-1} analysis, taking into account systematic uncertainties. We use the same event selection in this round of the analysis, and can be found in Table 6.

Variable	Untagged Channel	Tagged Channel
Two leptons	$m_{\ell\ell}$ >20 GeV	
Met Significance	> 4 GeV (for ee and $\mu\mu$: 76 GeV < $m_{\ell\ell}$ < 106 GeV)	
Top Killer A	215 GeV	
Top Killer B	325 GeV	
$\not\!\!E_T$	> 20 GeV	
$E_T^{jet_1}$	> 20 GeV	> 15 GeV
$E_T^{jet_2}$	>20 GeV	> 12 GeV
"L"-cut $\not\!\!E_T$	50 GeV	None
"L"-cut $\Delta\phi$	20^0	None

Table 6: Event selection cuts. See section 4.1 for Top Killer definition. $\not\!\!E_T$ is corrected for jets with $E_T \geq 12$ GeV, to level 5.

4.1 Top Killer

The dominant background for our search is $t\bar{t}$, especially in the tagged region. Due to heavier mass of the top quark, it has higher p_T final decay products. We found three kinematic variables reasonably discriminating between top and stop events: the scalar sum of all transverse final decay products momenta, H_T, and $\Delta\phi$ angles between two leptons and two jets in the event.

We found that one can obtain a fairly good discrimination between top and stop events in the two-dimensional plane of H_T vs $\Delta\phi\,(jets) \times \Delta\phi\,(leptons)$, as can be inferred from Figure 2. Placing a straight line cut

$$H_T < 215 + \frac{\Delta\phi\,(jet_0, jet_1)\,\Delta\phi\,(lep_0, lep_1)}{\pi^2} \times 325 \tag{8}$$

substantially reduces the number of top events, without hurting the acceptance for stop by too much. The top background is reduced by a factor of 2, while reducing stop by approximately 12%.

Figures 3 show data vs prediction comparison for the $\Delta\phi\,(jets)$, $\Delta\phi\,(leptons)$ and products of these two for events with 2 and more jets and $\not\!\!E_T > 20$ GeV.

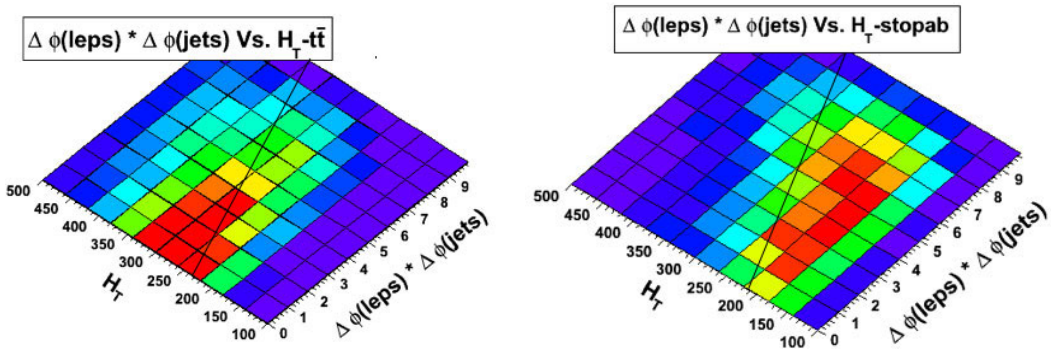

Figure 2: The H_T verses $\Delta\phi\,(leptons)\,\Delta\phi\,(jets)$ for top events (left), and stop events (right). It can been seen that stop events tend to lie at a lower H_T and larger $\Delta\phi_{\ell\ell}\Delta\phi_{jj}$. Making a diagonal cut in this plane efficiently removes top events, while keeping stops. The lines drawn correspond to $H_T = 215 + \frac{\Delta\phi(jet_0,jet_1)\Delta\phi(lep_0,lep_1)}{\pi^2} \times 325$

5 Monte Carlo Simulation

5.1 Stop Signal

For the stop signal simulation we generated several PYTHIA v6.216 samples. As an input to the MC generator we specify the stop mass, U(1) and SU(2) gaugino parameters (M_1 and M_2). The values M_1 and M_2 are approximately equal to neutralino ($\tilde{\chi}_1^0$) and chargino ($\tilde{\chi}_1^+$) masses. We also set the stop mixing angle to unity, and $\tan\beta = 5.0$. Note that the actual values of these two parameters are irrelevant, since they define mixing between light and heavy stop quarks, while the cross section of pair produced stop quarks does not depend on the mixing, but on the actual value of the stop mass only. Similarly, the actual relationships between $m_{\tilde{\chi}_1^+}$ and M_2, and between $m_{\tilde{\chi}_1^0}$ and M_1 are irrelevant, since masses of the supersymmetric particles will determine the acceptance and kinematics of the stop events.

5.2 Standard Model Backgrounds

For the background modeling we use the Top Group Monte Carlo samples [20]. We assume the world average value of top mass [21], and use 'ytop72' dataset as the nominal sample for $t\bar{t}$ events, while other top mass samples, as listed in Table 7, are treated as a systematics due to the uncertainty in the top mass value (see Sec. 6). We make use of inclusive diboson samples generated with PYTHIA v6.216, and $W\gamma$ samples generated with Baur by the electroweak group. The respective NLO cross sections for these physics processes are given in Table 7.

For Drell-Yan process modeling we use the Matrix Element ALPGEN v2.10 $Z/\gamma^\star \rightarrow \ell^+\ell^-$, $(\ell = e, \mu, \tau)$ events produced in association with light and heavy flavor jets.

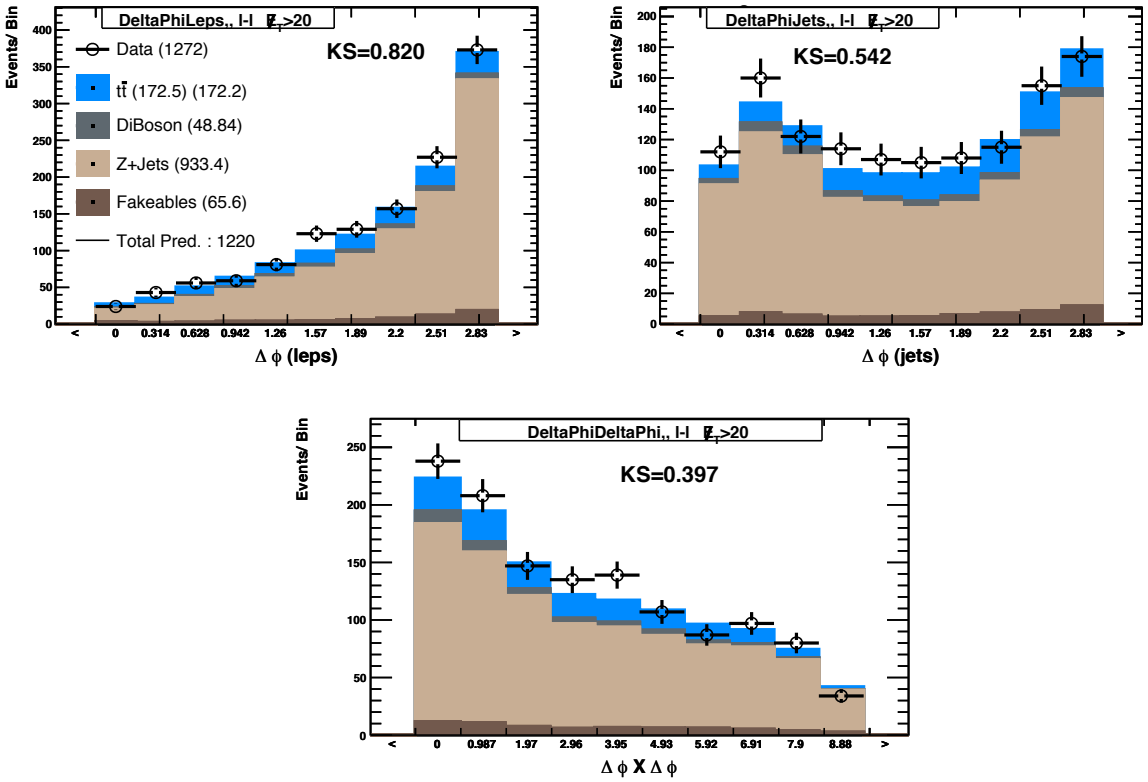

Figure 3: $\Delta\phi$ between jets (top left) $\Delta\phi$ between leptons (top right) and product of both (bottom) distributions in the $\geq$ 2-jet, $\not\!\!E_T > 20$ GeV region.

ALPGEN v2.10 uses PYTHIA v6.325 for parton shower simulation, and contains a built-in mechanism to remove the overlap between jets from parton showers and from

Physics Process	Generator	Dataset name	NLO Cross Section (pb)
$t\bar{t}$	PYTHIA	ytop72	7.23
$t\bar{t}$	PYTHIA	ttop75	6.7
$t\bar{t}$	PYTHIA	ttop70	7.8
WW	PYTHIA	itopww	12.4
WZ	PYTHIA	itopwz	3.7
ZZ	PYTHIA	itopzz	3.8
$W\gamma \to e\nu$	Baur	rewk38, 28	32×1.36
$W\gamma \to \mu\nu$	Baur	rewk39, 29	32×1.34
$W\gamma \to \tau\nu$	Baur	rewk2a,1a	32×1.36

Table 7: Non-Z SM Monte Carlo samples and their respective cross sections.

hard scattering matrix elements at the generator level ("MLM matching") [22] The samples with the largest parton multiplicities are generated using "inclusive" matching, allowing the parton shower to fill in additional jets. Other samples are generated with "exclusive" matching.

Since $Z/\gamma^\star$ events represent one of the major backgrounds for our analysis, we heavily suppress events with dilepton invariant masses inside of the Z mass peak region. (See Sec. 4). Therefore to increase statistics for events outside of Z mass peak region we also make use of ALPGEN samples with dilepton invariant masses generated outside of the Z mass. We generated samples with $20 < m_{\ell\ell} < 75$ GeV and $105 < m_{\ell\ell} < 600$ GeV in association with light and heavy flavor jets respectively.

The ALPGEN samples are merged according to their relative cross sections. The light-flavor events that also contain heavy flavors from the parton showers create an overlap between the light and heavy flavor samples that it is removed using the jet-based overlap removal scheme developed for the SECVTX top cross section analysis [23]. The scheme keeps $b\bar{b}$ and $c\bar{c}$ pairs in the light flavor sample only if they come from the parton shower and are contained in the same reconstructed jet ($\Delta R < 0.4$). In the heavy flavor samples, all events with $b\bar{b}$ and $c\bar{c}$ pair from the matrix element are kept if they do not share the same jet. We use $Z + b\bar{b}$ mc to account for both $Z + b\bar{b}$ and $Z + c\bar{c}$, events in the data, as we fit for the Z+HF scale factor separately from the Z+LF scale factor.

5.3 Luminosity Scaling

The MC samples listed in the previous sections are generated with run-dependent settings only up to integrated luminosities of 1.1 fb^{-1} (periods 0-8, runs 141544-22426). Therefore we re-scale the MC samples according to the full luminosity of the analyzed data sample. We follow the procedure outlined in Ref. [24]. We do one-to-one mapping for the data period 0, when the detector was not fully instrumented and for part of which the CMX triggering was missing, and re-weight the MC events from periods 1-8 to represent periods 1-17.

5.4 Tagging Efficiencies

The tagging efficiency is slightly lower in data than in the MC simulation. We correct for these discrepancies on a jet-by-jet basis. Heavy flavor jets in the MC simulation are identified by matching b and c hadrons from the list of observed particles (OBSP) within $\Delta R < 0.4$ to reconstructed jets in the event. In case of the match the jet is considered to be a heavy flavor jet, otherwise it is classified as a light flavor jet. Heavy flavor jets that are not b-tagged in the MC are considered untagged. For heavy flavor jets that are tagged we apply the SECVTX algorithm scale factor = 0.95 ± 0.05 [25]. For light flavor jets the tagging information from the MC is ignored, and the tagging efficiencies are obtained from the mistag matrix [25].

The MC event tagging efficiency is then calculated as the sum of all possible tagging combinations for jets in the event:

$$P_{event,tag} = 1 - \prod_j (1 - P_j), \tag{9}$$

where P_j is the jet tagging probability.

5.5 $Z/\gamma^\star \to \ell^+\ell^-$

5.5.1 NLO K-Factor

Since the ALPGEN is the LO matrix element generator, its cross sections for $Z/\gamma^\star \to \ell^+\ell^-$ production need to be corrected to account for NLO effects. We combine all monte carlo samples according to their relative cross sections and then normalize Monte Carlo to data in the Z mass peak region: 76 GeV $< m_{\ell\ell} <$ 106 GeV in the low missing E_T region: $\not\!\!E_T <$ 20 GeV. The K-factors for each ee or $\mu\mu$ dilepton category are presented in Table 8. For categories including CMX muon only events with at least one jet $E_T >$ 15 GeV are considered, since for some periods of time data has been collected on CMX+JET10 trigger (see Sec. 3.1).

The overall K-factor for the $Z/\gamma^\star \to \ell^+\ell^-$ events is obtained by combining all of the dilepton categories and is found to be equal to 1.44. The total uncertainty applied for the total $Z/\gamma^\star \to \ell^+\ell^-$ normalization is discussed in the next section.

5.5.2 N_{jet} Scale Factors

Although the ALPGEN generator takes care of the correct matrix element treatment for $Z/\gamma^\star \to \ell^+\ell^-$ production in association with jets, the jet multiplicity distribution does not agree with data perfectly. It was noted that the agreement can be improved if one shifts the Q^2 or the JES scale [24]. Instead we apply the N_{jet} scale factors relative to the global K-factor obtained in previous section to correct for the number of $Z/\gamma^\star \to \ell^+\ell^-$ events per each jet multiplicity bin: 0, 1 and $\geq$ 2. The N_{jet} scale factor in general depends on the jet energy thresholds. Table 9 shows the N_{jet} scale factors for the leading jet $E_T >$ 15 GeV, and the second jet $E_T >$ 12 GeV. The third row represents the N_{jet} scale factor for combined $ee + \mu\mu$ events, and a half of the discrepancy between ee and $\mu\mu$ channels is added in quadrature to the statistical uncertainty of the fit.

5.5.3 Heavy Flavor Scale Factor

ALPGEN is known to under-predict data in the low-multiplicity bins in the $\geq$ 1 SECVTX tag region for both W and Z + heavy flavor events [23, 26]. To account for that we calculate additional jet bin-by-bin heavy flavor scale factors inside of the Z mass peak, low missing E_T region as in Sec. 5.5.1. Approximately half of the contribution to the tagged region comes from Z + light flavor jets, where one or more of light flavor jets are mis-tagged. Since the mistag matrix is obtained from data and used in other CDF analyses we assume that it gives the correct scaling for Z + light

flavor events. On the other hand the NLO K-factor for Z + heavy flavor events can be distinct from the one for Z + light flavor events. Based on these arguments we scale up only Z+heavy flavor contribution to match the data. Like the Z + light flavor scale factor, we obtain the Z+heavy flavor scale factor inside of the Z mass peak, and use this to extrapolate outside of the Z mass peak. Due to technical difficulties we were

Dilepton Category	K-factor
CEM_CEM	1.44 ± 0.01
CEM_NICEM	1.54 ± 0.03
CEM_PHX	1.40 ± 0.01
PHX_NICEM	1.45 ± 0.03
CMUP_CMUP	1.49 ± 0.01
CMUP_NICMUP	1.82 ± 0.07
CMUP_CMU	1.56 ± 0.02
CMUP_NICMU	1.98 ± 0.14
CMUP_CMP	1.48 ± 0.02
CMUP_NICMP	1.75 ± 0.12
CMUP_CMX	1.52 ± 0.03
CMUP_NICMX	1.76 ± 0.10
CMX_NICMUP	1.89 ± 0.11
CMUP_CMIO	1.38 ± 0.02
CMX_CMX	1.38 ± 0.04
CMX_NICMX	1.46 ± 0.12
CMX_CMU	1.51 ± 0.06
CMX_NICMU	1.85 ± 0.23
CMX_CMP	1.37 ± 0.05
CMX_NICMP	1.35 ± 0.17
CMX_CMIO	1.43 ± 0.07
All_Leptons	1.44 ± 0.01

Table 8: NLO K-factors for various dilepton categories. Errors are statistical only.

	0j	1j	$\geq$ 2j
ee	0.983 ± 0.003	0.937 ± 0.008	1.178 ± 0.016
$\mu\mu$	1.021 ± 0.007	1.015 ± 0.011	1.189 ± 0.018
Total	0.992 ± 0.019	0.969 ± 0.040	1.182 ± 0.011

Table 9: Jet bin correction factors for Z events obtained within the Z mass peak region 76 GeV $< m_{\ell\ell} <$ 106 GeV relative to the total K-factor = 1.44. The uncertainty on the total scale factor takes into account statistical uncertainty added in quadrature to half of the discrepancy between ee and $\mu\mu$ channels.

not able to generate the Drell-Yan + $c\bar{c}$ events below the Z mass peak region, therefore since the event kinematics of $Z/\gamma^\star + c\bar{c}$ and $Z/\gamma^\star + b\bar{b}$ are the same and only differ by b-tagging probabilities, we use the $Z/\gamma^\star + b\bar{b}$ monte carlo to represent Z + heavy flavor events, sine we fit for the Z + heavy flavor scale factor. The heavy flavor scale factors using jet thresholds 15 GeV for the leading and 12 GeV for the second jet is computed without $Z + c\bar{c}$ contribution and are given in Table 10, and used in this analysis.

	1j	$\geq$ 2j
ee	2.31 $\pm$ 0.10	1.44 $\pm$ 0.10
$\mu\mu$	2.90 $\pm$ 0.11	1.43 $\pm$ 0.10
Total	2.57 $\pm$ 0.15	1.44 $\pm$ 0.07

Table 10: Jet bin correction factors for Z + heavy flavor events without $Z + c\bar{c}$ events. The uncertainty on the total scale factor takes into account statistical uncertainty added in quadrature to half of the discrepancy between ee and $\mu\mu$ channels.

5.6 Fake Lepton Background

Events from $t\bar{t} \to \ell$ + jets, W+jets and QCD processes, where one or more jets fake a lepton, can also contribute to our data sample. We model the fake lepton background with data using a procedure similar to Ref. [18]

We define fakeable lepton objects for each lepton category as specified in Tables 11 and 12. We require that the real identified leptons are not part of fakeable objects for reasons described below. To estimate the fake lepton background we choose events with one fully identified lepton, and one or more fake leptons. We treat the fake lepton as if it was a fully identified lepton, but the event will contribute to the background template with a weight (fake rate f_i), which is a function of lepton type, and lepton p_T The fake rates are calculated using the QCD data collected with JET_50 trigger. Fake rates are defined as

$$f_i = N_{lep,i}/N_{fakeable,i}, \tag{10}$$

and computed per each i-th lepton p_T bin: [20-30],[30-40], [40-60], [60-100], [100-200] and $\geq$ 200 GeV. In calculation of the fake rate matrix only one fakeable was allowed per event. Photon conversions and cosmic muons were removed. We require the corrected $\not\!\!E_T$ and candidate lepton to have a transverse invariant mass less than 25 GeV to help reduce the contributions from W events. The contributions from W and Z that contain real leptons were found to be negligible [18].

Fakeable (NI)CEM	Fakeable PHX
$E_T \geq 20$ GeV	$E_T \geq 20$ GeV
Photon Conversion Veto	Match to Phoenix Track
Iso($\Delta R = 0.4/E_T$) ≤ 0.1 (unless NI)	Iso($\Delta R = 0.4/E_T$) ≤ 0.1
$E_{had}/E_{em} \leq 0.125$	$E_{had}/E_{em} \leq 0.125$
+ at least one anti-cut:	
$E_{had}/E_{em} \geq 0.055 + 0.00045E$	$E_{had}/E_{em} \geq 0.05$
$\chi^2_{CES} \geq 10$	
$L_{shr} \geq 0.2$	$\chi^2_{PEM} \geq 10$
$\lvert\Delta z_{CES}\rvert \geq 3$ cm	PES 5×9 U ≤ 0.65
-3 cm $\geq Q \times \Delta x_{CES}$, $Q \times \Delta x_{CES} \geq 1.5$ cm	PES 5×9 U ≤ 0.65

Table 11: Electron Fakeables Selection Criteria

(NI) (CMUP / CMU / CMP)	(NI)CMX	CMIO
$p_T \geq 20$ GeV/c		
Ax SLs with 5 hits/SL ≥ 3		
St SLs with 5 hits/SL ≥ 2		
Track $\lvert z_0\rvert \leq 60$ cm		
$d_0 <$ (w/Si Hits 0.02, w/o 0.2) cm		
Iso($\Delta R = 0.4/E_T$) ≤ 0.1 (unless NI)		
$E/p < 1$		
No match to CDF Em Object		
Fiducial to CES		
Fiducial $x_{CMUP,CMU,CMP} < 0$ cm	Fiducial $x_{CMX} < 0$ cm	Non-fudical
Fiducial $z_{CMUP,CMU} < -3$ cm	Fiducial $z_{CMX} < -3$ cm	Non-fudical
Fiducial $z_{CMP} < 0$ cm		Non-fiducial
+ at least one anti-cut:		
$E_{em} >$ 2 GeV + max(0,0.0115*(p-100))		
$E_{had} >$ 6 GeV + max(0,0.028*(p-100))		
No Stub	No Stub	
$\lvert\Delta x_{CMU}\rvert > 7$ cm (for CMUP,CMU)	$\lvert\Delta x_{CMX}\rvert > 6$ cm	$E_{em} + E_{had} \leq 0.1$
$\lvert\Delta x_{CMP}\rvert > 5$ cm (for CMUP,CMP)		

Table 12: Fakeable Muon Selection Criteria

6 Systematic Uncertainties

6.1 Jet Energy Scale

To account for uncertainties in the measured jet energies, we shift energies of the jets up and down by $\pm 2\sigma$ of their jet energy resolutions and re-run the stop mass reconstruction algorithm. Thus we obtain the mass templates corresponding to the shifted jet energy scale. We also account for the shape changes due to events moving in and out because of the JES shift and evaluate the relative change in acceptance.

The jet energy scale enters into our likelihood fit as a Gaussian constraint nuisance parameter. To obtain the JES template corresponding to the value of the nuisance parameter between 0 and +(-) 2 σ, we interpolate the nominal and +(-) 2 σ JES templates using the horizontal morphing technique. To account for the rate and proper normalization of the template due to the shift, we linearly interpolate acceptance values corresponding to nominal and +(-) 2 σ acceptances, and re-normalize the template respectively.

For Z+Jet the normalization procedure in section 5.5.2 is re-performed at +(-) 2 σ JES, and these resulting normalization factor are used for the JES varied Z+Jet templates in the signal region.

This systematics is not applied to fake lepton background, since it is obtained from data.

6.2 Z+Jets Normalization

We take a rate uncertainty for normalization of Z +jets background in the Z mass: $76 < m_{\ell\ell} < 106$ GeV, $\not\!\!E_T < 20$ GeV region, as an uncertainty for the N_{jet} scale factor in the ≥ 2 jets bin (see Sec. 5.5.2) For this set of cuts, where the leading jet $E_T > 15$ GeV and the second jet $E_T > 12$ GeV, it is equal to 1.1%.

6.3 Z+Heavy Flavor Jets Normalization

Similarly , we take a rate uncertainty for normalization of Z +heavy flavor jets background in the Z mass: $76 < m_{\ell\ell} < 106$ GeV, $\not\!\!E_T < 20$ GeV region, as an uncertainty for the heavy flavor scale factor in the ≥ 2 jets bin (see Sec. 5.5.3) For set of cuts, where the leading jet $E_T > 15$ GeV and the second jet $E_T > 12$ GeV, it is equal to 7.2%.

6.4 B-Tagging

To estimate systematic uncertainties due to the SECVTX b-tagging algorithm, we vary the per-jet tagging probability by $\pm 1\sigma$ [25]. The tagging probabilities for heavy flavor jets and light flavor mistags are varied independently. We also take into account migrations of events between the untagged and the tagged channels. We apply only a rate uncertainty for this systematic.

Since Z + heavy flavor rate is normalized to data, its uncertainty already incorporates the uncertainties due to b-tagging algorithm. Therefore to avoid double counting of systematics, we explicitly don't apply b-tagging uncertainty to Z + heavy flavor events. Additionally, since the fake lepton background is derived from data, B-Tagging uncertainty is not applicable to this background.

6.5 Lepton ID/Trigger Efficiencies

Statistical uncertainties on trigger efficiencies and lepton scale factors are taken as systematics. They converted into uncertainties per each dilepton category, and assumed to be fully correlated between MC based samples. The statistical uncertainties due to these effects is found to be 0.4%. However, in comparing predicted Z event yield in each dilepton category to data, it was seen that this was possible an underestimate of the error. Instead we use the weighted fractional difference between the predicted and observed number of events, for each dilepton category, to find an error of 1.2% due to trigger and lepton id scale factor errors. This uncertainty is not applied to the $Z + Jets$ background since it is normalized using the data, or fake lepton background, since it is data derived.

6.6 Fake Lepton Uncertainty

To estimate the uncertainty on the fake lepton background we repeat the exercise in section 5.6, but instead using QCD data from JET_20 and JET_70 triggers. To estimate the systematic uncertainty on our fake predictions we take a fake matrix computed from a sample JET_X and apply it to a sample JET_Y, and compare the predicted number of identified leptons, to actual number of identified leptons in that jet sample, neglecting any real lepton contamination.

JET_20 rates applied to JET_50 sample
Predicts 9087 leptons, observe 7681. An 18.3% over prediction
JET_70 rates applied to JET_50 sample
Predicts 7854 leptons, observe 7681. An 2.3% over prediction
JET_50 rates applied to JET_20 sample
Predicts 4653 leptons, observe 5116. An 9.0% under prediction
JET_50 rates applied to JET_70 sample
Predicts 1070 leptons, observe 1014. An 5.6% over prediction

Additionally, using the fake rates from JET_20 to predict the lepton plus fakeable background predicts 3.5% less and 21.0% more events in the tagged and anti-tagged signal regions respectively. For JET_70 it is 2.0% and 4.1% more events for the tagged and anti-tagged signal region respectively.

However since the fake lepton background uncertainty has little effect on our limits we choose to use the historically used rate uncertainty of 30% for this background in

this analysis.

6.7 Top Mass

We use the top mass world average value of 172.5 ± 1.5 GeV [21], for which corresponding $t\bar{t}$ cross section is 7.23 pb [33]. We use three top mass points: 170, 172.5, and 175 GeV, and create the reconstructed stop mass templates for each top mass sample. We use the top mass as a nuisance parameter in our likelihood fit, and linearly interpolate the templates corresponding to different top mass points accounting for normalization due to acceptance changes and variation of the $t\bar{t}$ cross section, as well as shape differences, with the top mass.

6.8 Initial/Final State Radiation

For both top and stop signal we simultaneously vary the amount of ISR and FSR. We generated the ISR/FSR less and ISR/FSR more samples for different stop mass points and use $t\bar{t}$ MC samples with ISR/FSR less (dataset: otopo4) and ISR/FSR more (dataset: otopo3) generated by the Top Group [20]. We take this systematic into account as both the rate and shape uncertainty by interpolating stop and top templates, and using an amount of the ISR/FSR as a nuisance parameter in the likelihood. Since the ISR/FSR samples for top are not generated for our nominal value of the top mass, we use compound morphing (see Sec. 10) to interpolate ISR/FSR templates for m_t=175 GeV point first, and then morph it to the value of m_t used in the fit.

6.9 Luminosity

The integrated luminosity uncertainty of 5.9% [35] is only applicable to $t\bar{t}$, stop and diboson sources, and only as a rate uncertainty.

6.10 Theoretical Cross Section

We take into account the uncertainties in the NLO theoretical cross section calculations for $t\bar{t}$, stop and diboson events and apply them as rate uncertainties. The uncertainty for combined diboson processes is 10%, and is taken as uncorrelated with any other systematics.

The uncertainty in $t\bar{t}$ and stop pair production cross sections can be separated into the uncertainty due to Q^2 scale and the uncertainty due to parton distribution functions. For the $t\bar{t}$ pair production it is 7% each. For the stop production the uncertainties are larger: 11% due to Q^2 (see Table 1) and 14% due to PDFs [36]. We take the uncertainties due to PDFs correlated between top and stop, while treat uncertainties due to Q^2 as uncorrelated.

7 Control Regions Validation

We sub-divide the phase space of dilepton events into various regions and in each of them make comparisons of the total predicted number of events with the number of observed events and also compare kinematic distributions. We require that two leptons are well separated: $\Delta R > 0.4$ and $m_{\ell\ell} > 20$ GeV. We analyze individually each jet multiplicity bin: 0, 1 or ≥ 2; separate events into bins of low missing E_T ($\not\!\!E_T < 20$ GeV) or high missing E_T ($\not\!\!E_T > 20$ GeV), tagged or pretag, and opposite vs same-sign charged leptons. For each of these control regions in this note we present distributions of leading and second lepton p_T, dilepton invariant mass and $\not\!\!E_T$ distributions.

7.1 Pre-Tag Region

In the pre-tag, the agreement in low missing E_T region is sufficient for this analysis, as evidenced in Figures 4-7 . Also shown in Figures 8-11 is the high *met* region, although this is not a true control region it can be seen the modeling is quite accurate.

7.2 B-Tagged Region

Figures 13-16 show we can accurately model B-Tagged control regions, as well higher $\not{E}_T$ regions (were signal would still be negligible).

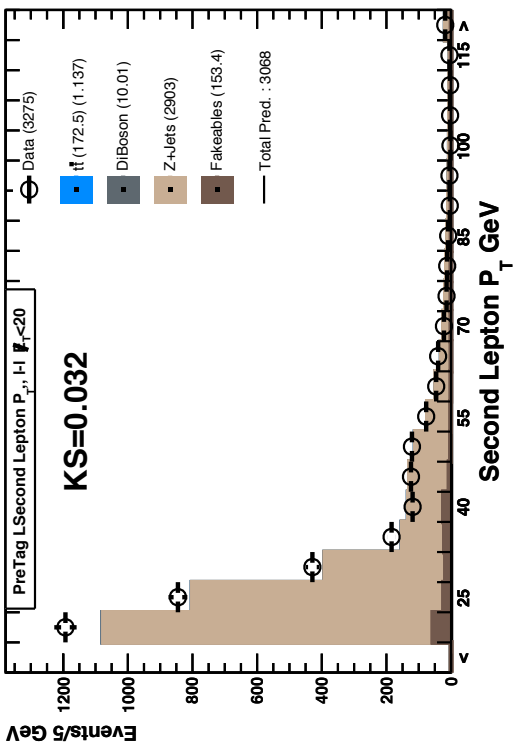

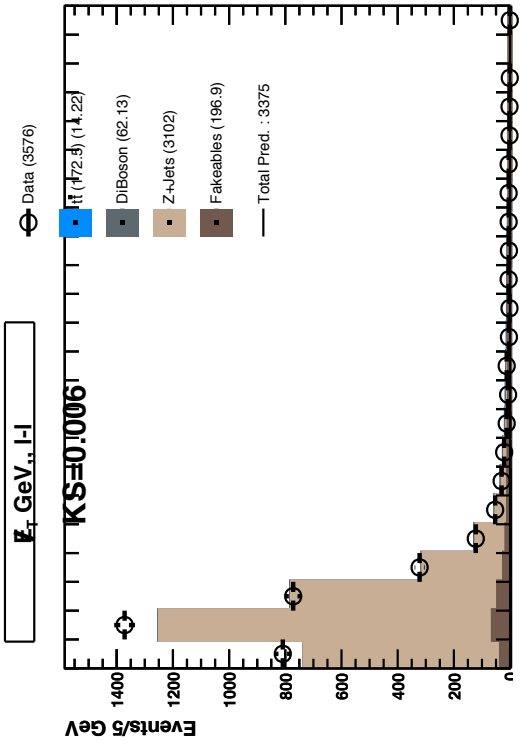

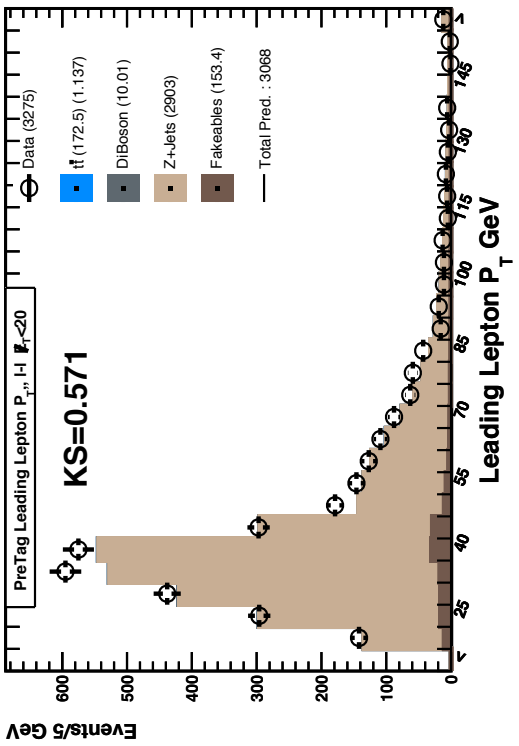

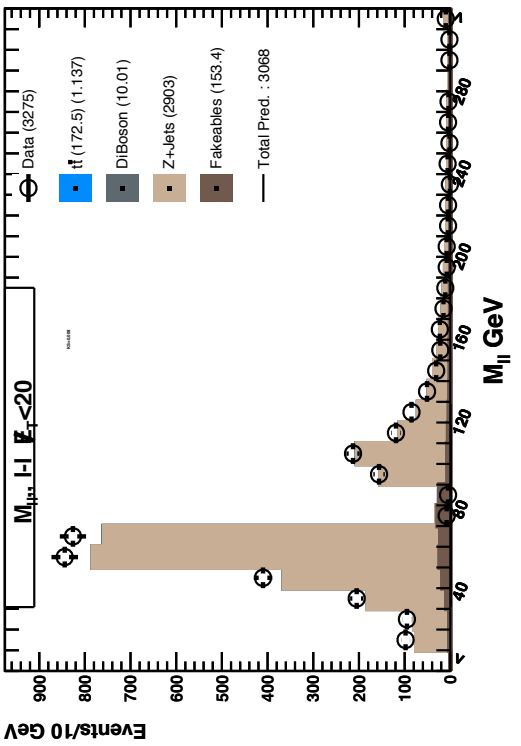

Figure 4: Pre-Tag, Opposite-sign events, $\not\!\!E_T < 20$ GeV, 1 jet Bin, Met Significance > 4 GeV for ee and $\mu\mu$: 76 GeV $< m_{\ell\ell} < 106$ GeV

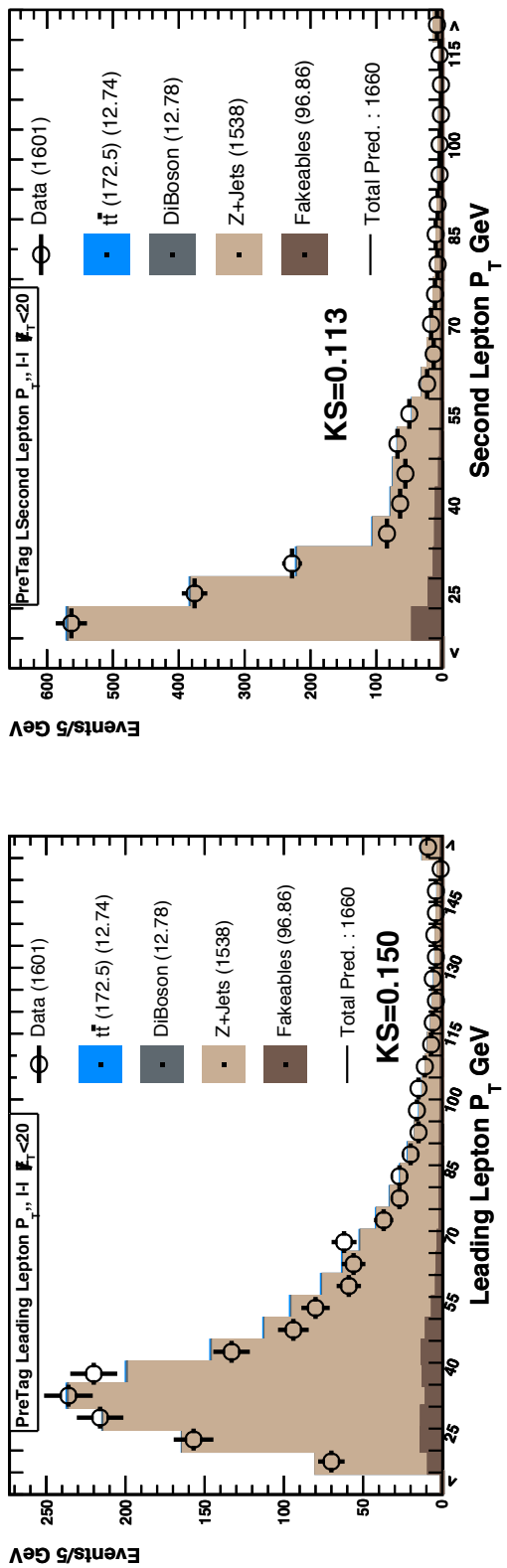

Figure 5: Pre-Tag, Opposite-sign events, $\not\!\!E_T < 20$ GeV, ≥ 2 jet Bin, Met Significance > 4 GeV for ee and $\mu\mu$: 76 GeV $< m_{\ell\ell} < 106$ GeV

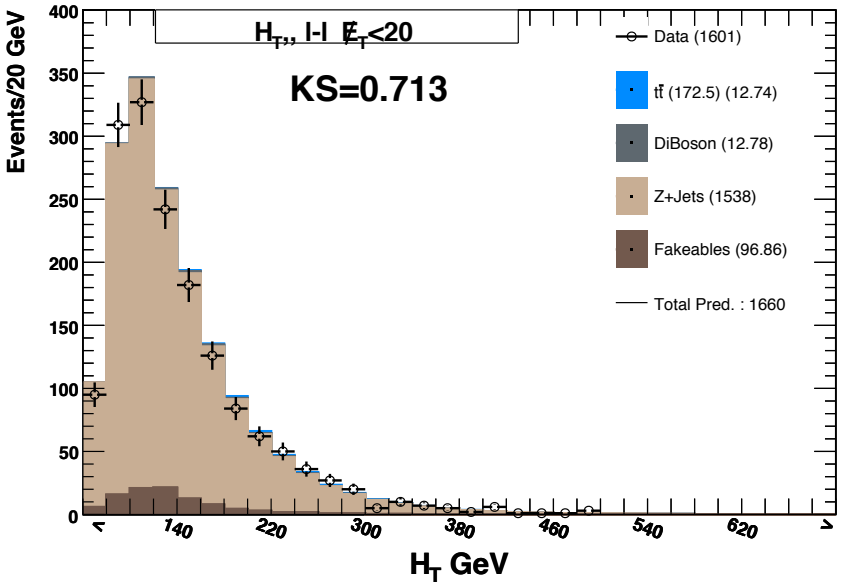

Figure 6: H_T of the second jet in Pre-Tag, Opposite-sign events, $\not\!\!E_T < 20$ GeV, ≥ 2 jet, Met Significance > 4 GeV for ee and $\mu\mu$: 76 GeV $< m_{\ell\ell} <$ 106 GeV

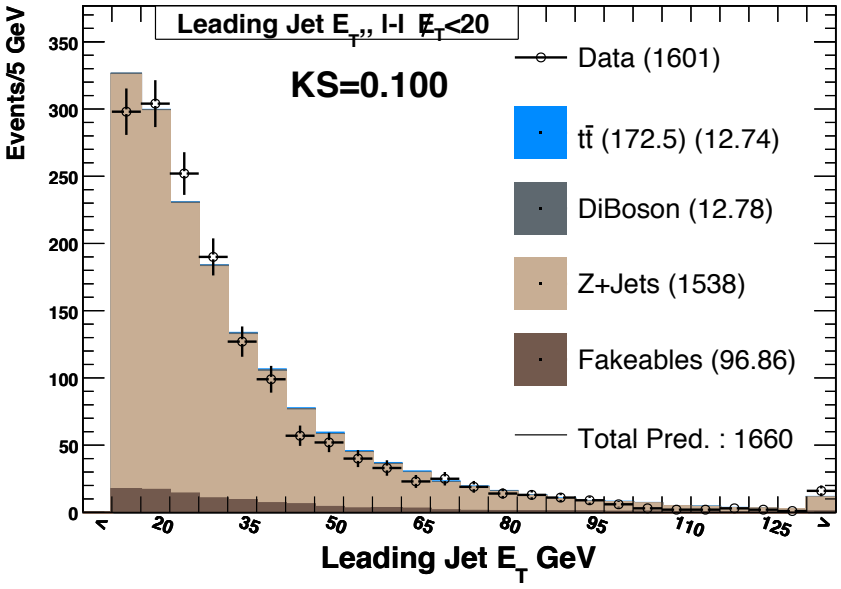

Figure 7: E_T of the leading jet in Pre-Tag, Opposite-sign events, $\not\!\!E_T < 20$ GeV, 1 jet Bin, Met Significance > 4 GeV for ee and $\mu\mu$: 76 GeV $< m_{\ell\ell} <$ 106 GeV

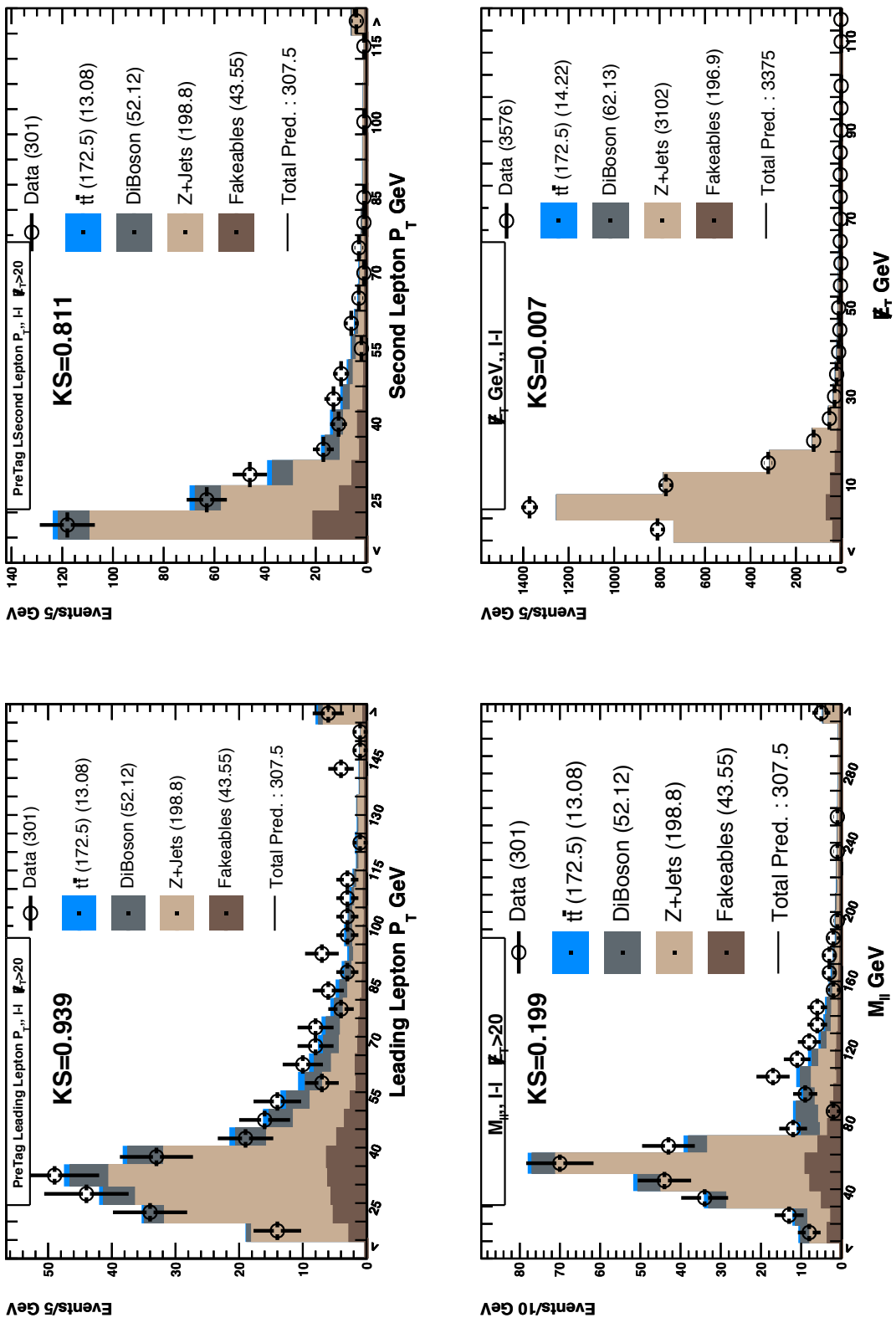

Figure 8: Pre-Tag, Opposite-sign events, $\not\!\!E_T > 20$ GeV, 1 jet Bin, Met Significance > 4 GeV for ee and $\mu\mu$: 76 GeV $< m_{\ell\ell} < 106$ GeV

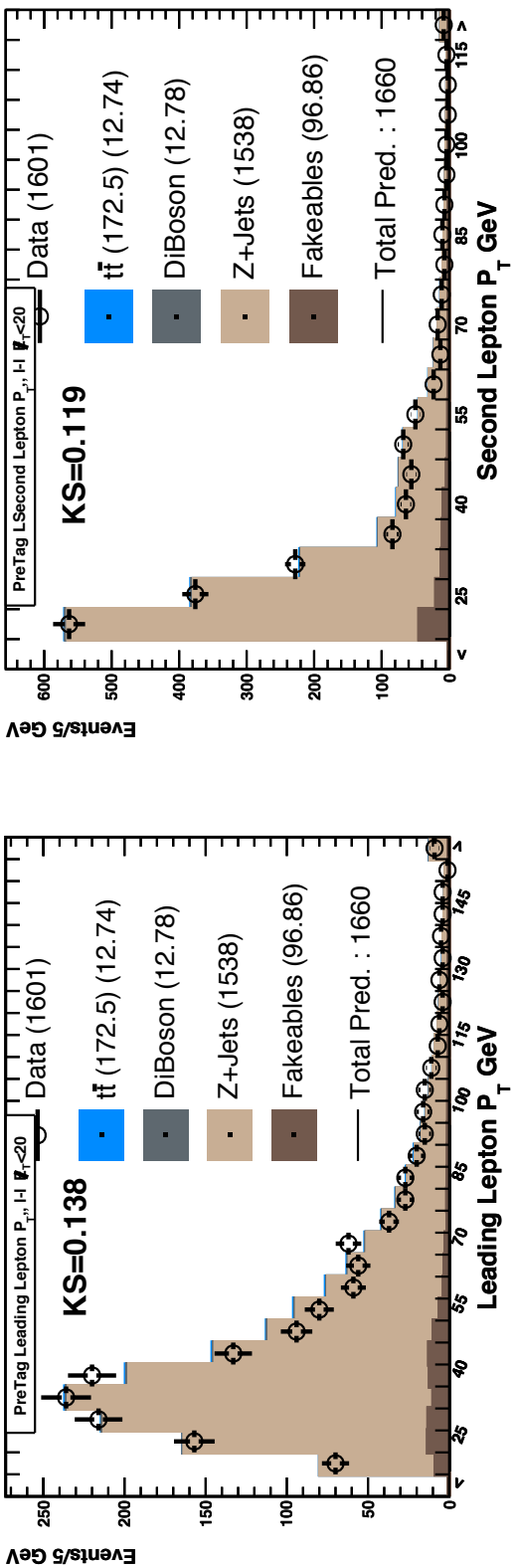

Figure 9: Pre-Tag, Opposite-sign events, $\not\!\!E_T > 20$ GeV, ≥ 2 jet Bin, Met Significance > 4 GeV for ee and $\mu\mu$: 76 GeV $< m_{\ell\ell} < 106$ GeV

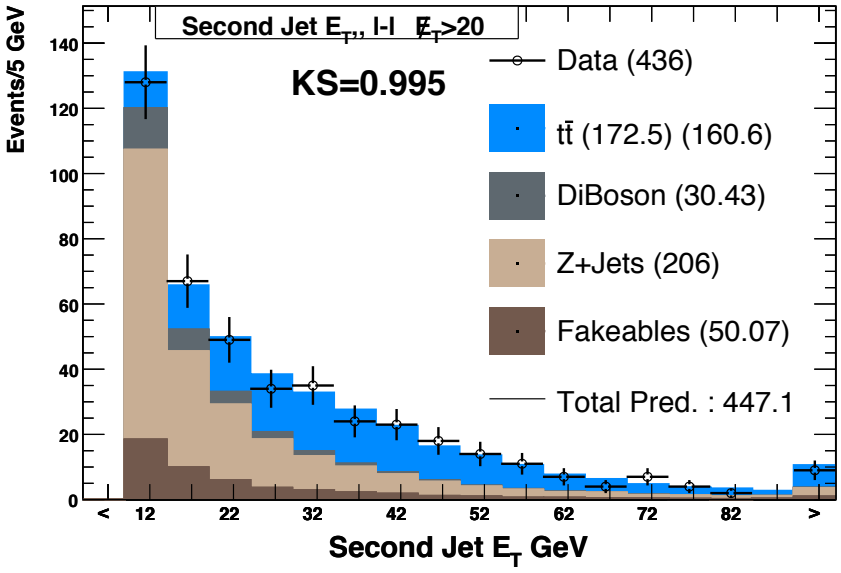

Figure 10: E_T of the second jet in Pre-Tag, Opposite-sign events, Met Significance > 4 GeV for ee and $\mu\mu$: 76 GeV $< m_{\ell\ell} <$ 106 GeV

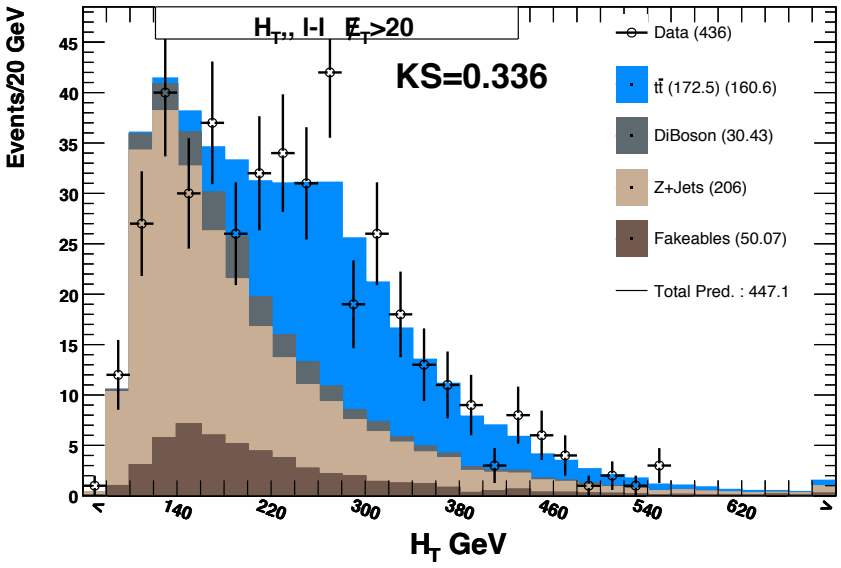

Figure 11: H_T of the second jet in Pre-Tag, Opposite-sign events, ≥ 2 jet, $\not\!\!E_T > 20$ GeV, Met Significance > 4 GeV for ee and $\mu\mu$: 76 GeV $< m_{\ell\ell} <$ 106 GeV

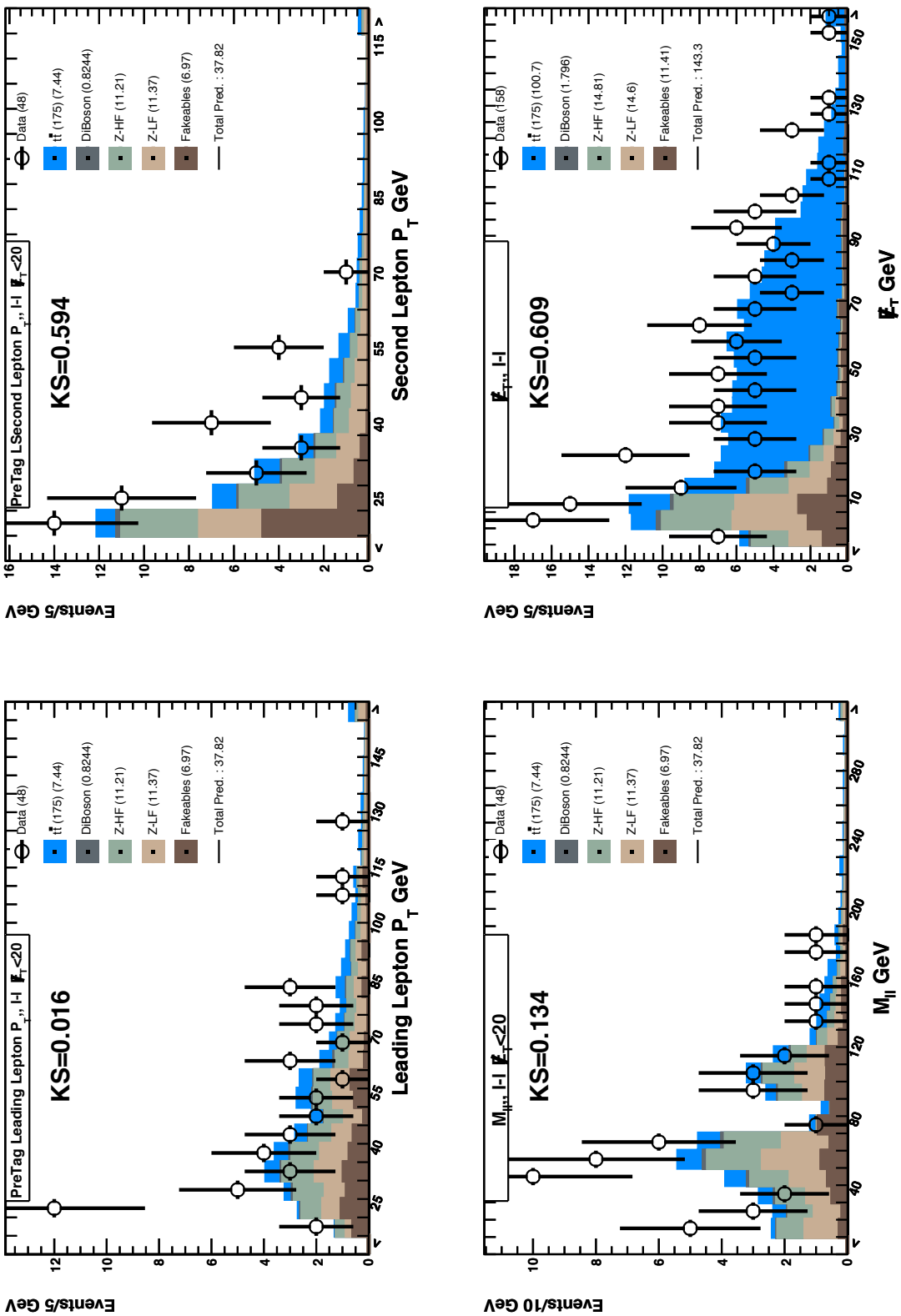

Figure 12: B-Tagged, Opposite-sign events, $\not\!\!E_T < 20$ GeV, ≥ 2 jet Bin, Met Significance > 4 GeV for ee and $\mu\mu$: 76 GeV $< m_{\ell\ell} < 106$ GeV

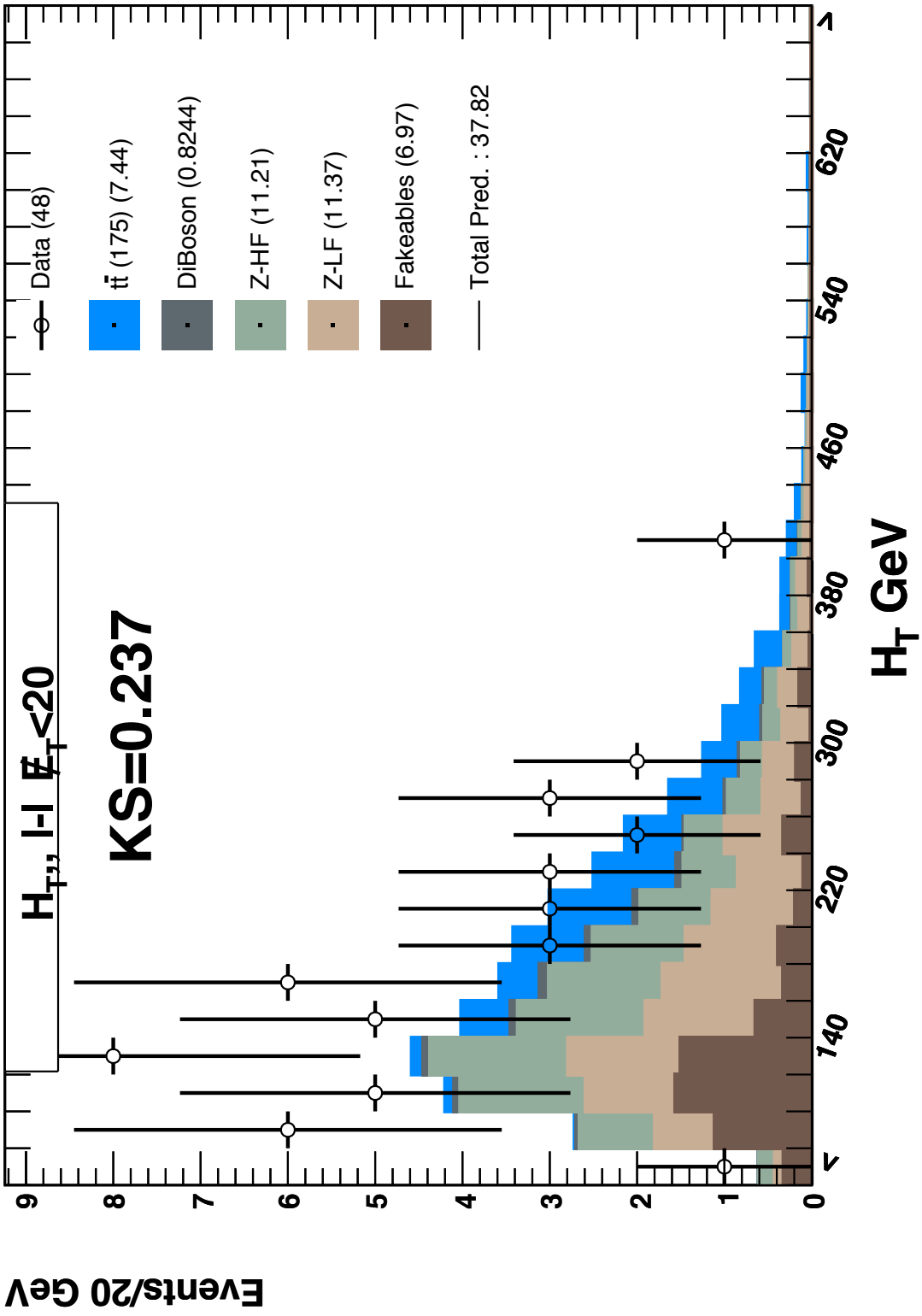

Figure 13: H_T of B-Tagged, Opposite-sign events, $\not\!\!E_T < 20$ GeV, ≥ 2 jet Bin, Met Significance > 4 GeV for ee and $\mu\mu$: 76 GeV $< m_{\ell\ell} <$ 106 GeV

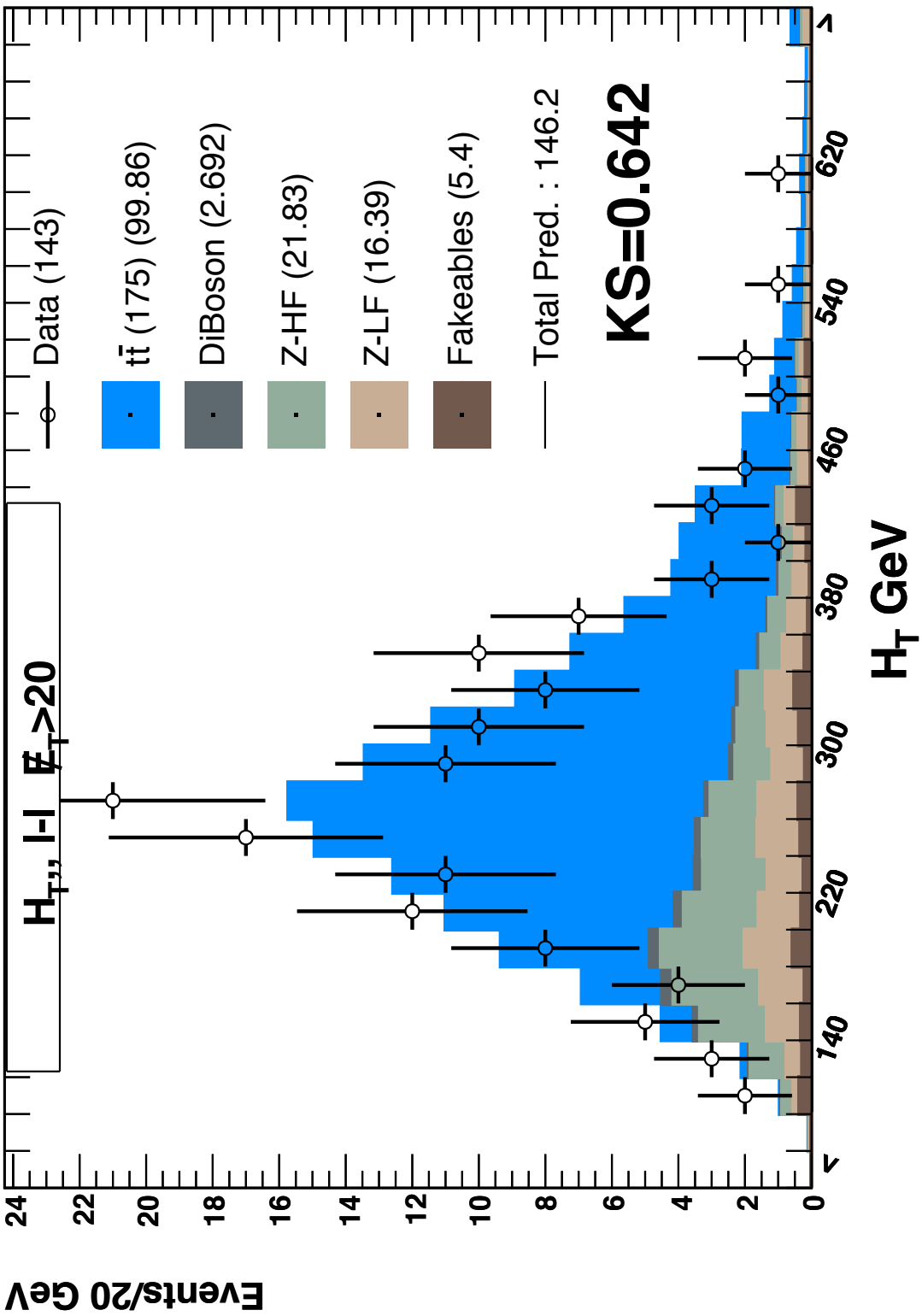

Figure 14: B-Tagged, Opposite-sign events, $\not\!\!E_T > 20$ GeV, ≥ 2 jet Bin, Met Significance > 4 GeV for ee and $\mu\mu$: 76 GeV $< m_{\ell\ell} < 106$ GeV

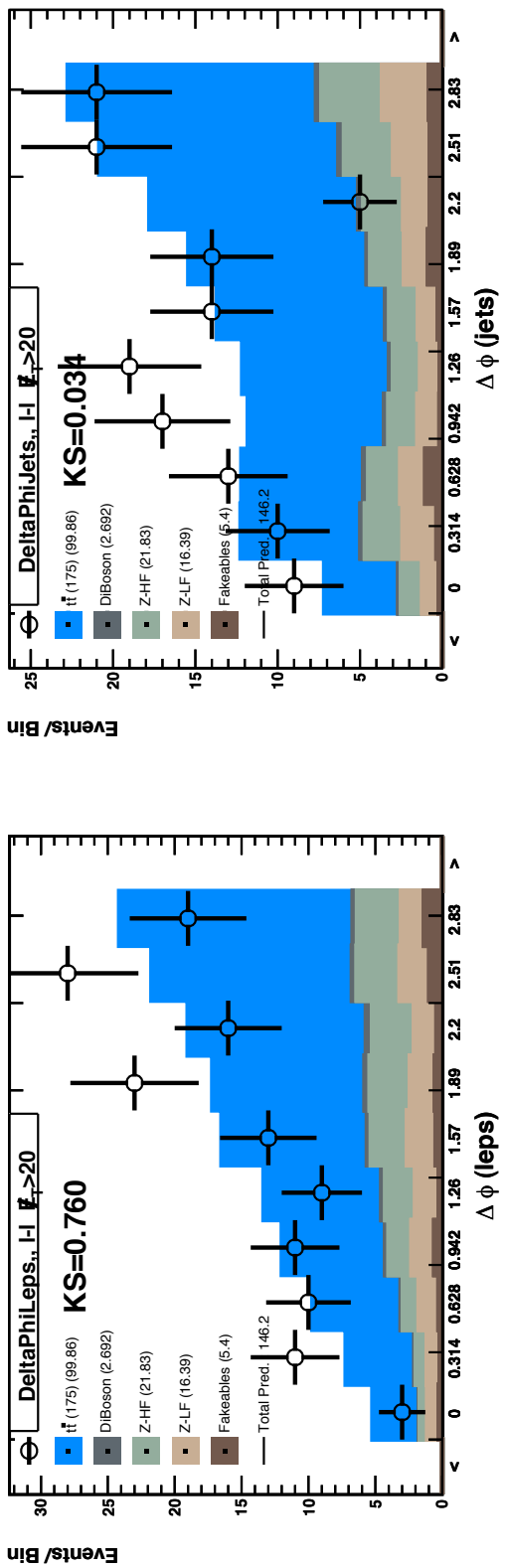

Figure 15: B-Tagged, Opposite-sign events, $\not\!\!E_T > 20$ GeV, ≥ 2 jet Bin, Met Significance > 4 GeV for ee and $\mu\mu$: 76 GeV $< m_{\ell\ell} < 106$ GeV

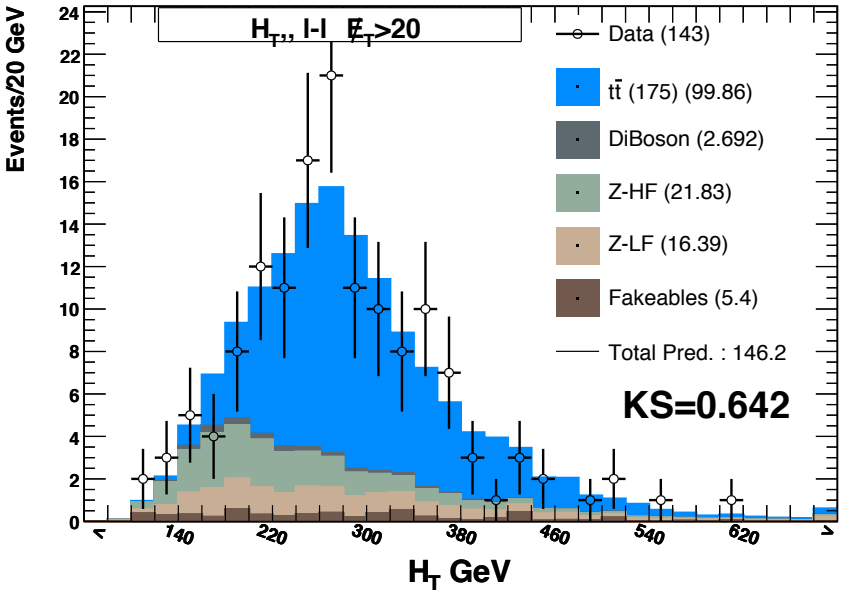

Figure 16: H_T of B-Tagged, Opposite-sign events, $\not\!\!E_T > 20$ GeV, ≥ 2 jet Bin, Met Significance > 4 GeV for ee and $\mu\mu$: 76 GeV $< m_{\ell\ell} <$ 106 GeV

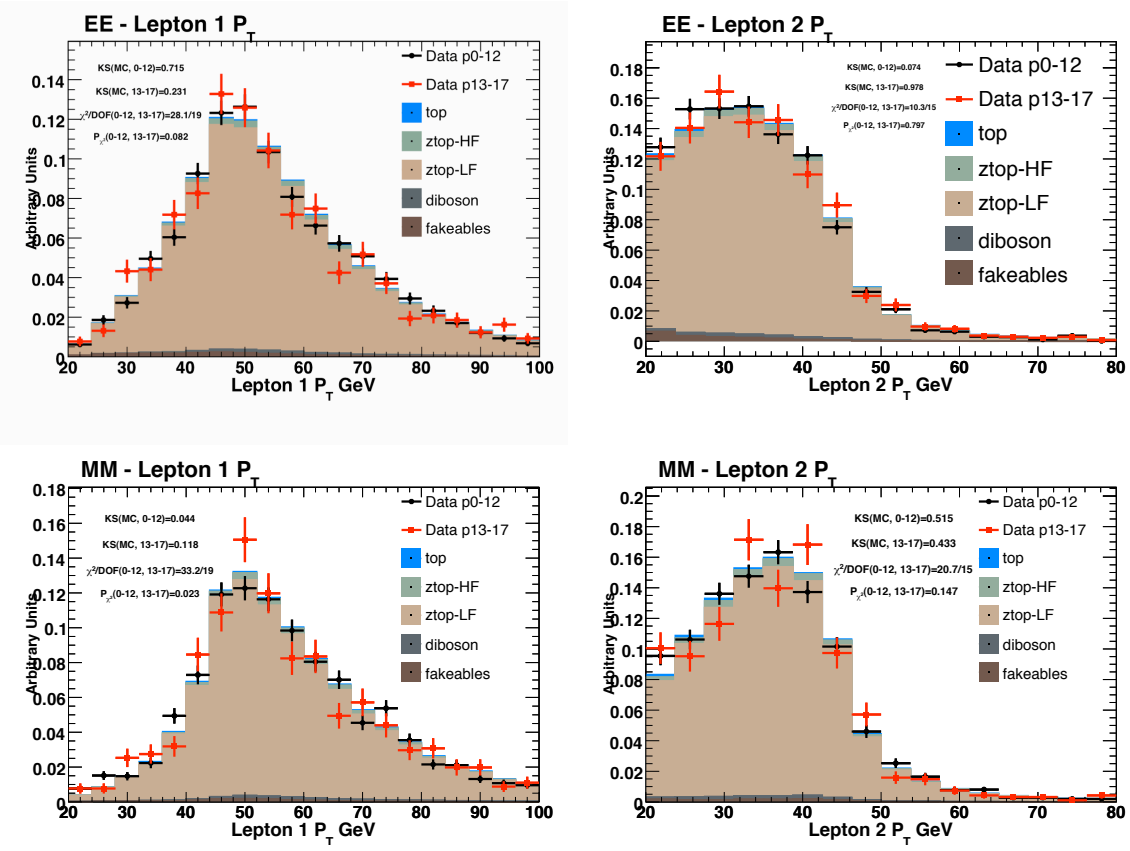

Figure 17: Lepton P_T for ee (top) and $\mu\mu$ (bottom) data event, for both the leading p_T (left) lepton, and the second lepton (right). These correspond to Opposite-sign events with ≥ 2 jets.

8 Period 13-17 data validated against periods 0-12 data

Below compare period 0-12 data, used for the first version of this analysis, to data collected since then, 13-17. As can be seen from Figures 17-21, there were no major changes in the data that greatly effect this analysis.

9 Stop Mass Reconstruction

Given our desire to set smooth confidence limits in SUSY mass space, rather than just setting limits for discreet points corresponding to the MC we generated, we need a single discriminating variable, thus we cannot use a Neural Network, or some other multivariate technique that is highly dependent on event kinematics, since these vary

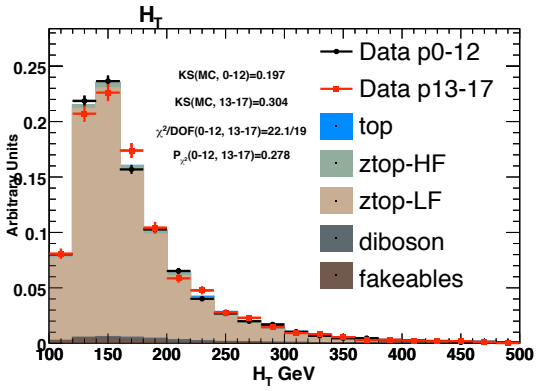

Figure 18: h_T for Opposite-sign events, with ≥ 2 jets

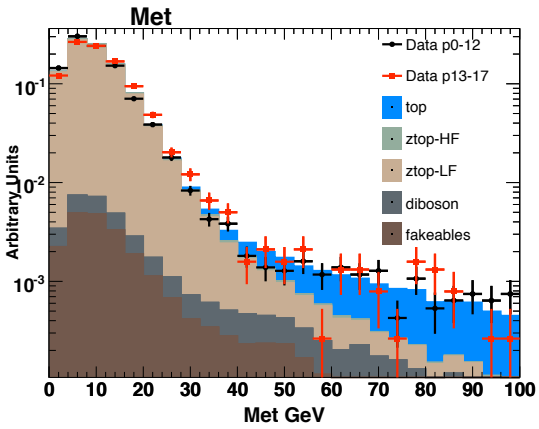

Figure 19: $\not\!\!E_T$ for Opposite-sign events, $\not\!\!E_T > 20$ GeV, with ≥ 2 jets

depending on SUSY masses. Full reconstruction of the stop events is used to obtain a single highly-discriminating variable between stop events corresponding to various SUSY mass points and the Standard Model backgrounds.

Dilepton stop decays produce four observable particles in the final state plus the missing energy due to additional four undetected neutrinos and neutralinos. This leads to a severely under-constrained system of particle four-momenta equations, making event reconstruction very challenging. However, through the use of a few approximations and assumptions on the $\tilde{\chi}_1^{\pm}$ masses as described below, we can do quite a decent job of reconstructing the original stop quarks kinematics and mass. A more complete description of stop event reconstruction can be found in [6], but a summary is given below.

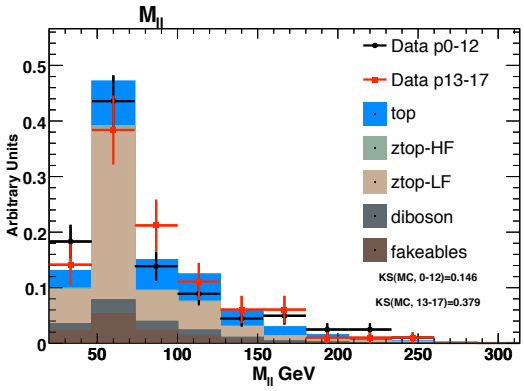

Figure 20: m_{ll} for Opposite-sign events, with ≥ 2 jets, $met > 20$ GeV, and passing the Top Killer cut

9.1 Pseudo-Particle Approximation

One of the most important approximation we make is combining four-momenta of $\tilde{\chi}_1^0$ and ν coming from each $\tilde{t}_1$ together and treat them as one massive Pseudo-Particle, as can be justified from 22.

9.2 Jet-To-Parton Assignment

To successfully reconstruct the stop mass we must accurately assign the $b(\bar{b})$ and the proper lepton. We use logic based on jet-lepton invariant mass quantities and successfully pair the correct jet-to-lepton 85% to 95% of the time, when both b-jets are in the leading two jets of the event.

9.3 Weighting Method

After making the Pseudo-Particle approximation and placing the $\tilde{\chi}_1^{\pm}$ - mass constraint, the event kinematics is still under-constrained (a -1C system), such that it is not possible to reconstruct kinematics of the event uniquely. We develop the method similar to the top dilepton neutrino weighting technique [9]. For a given Pseudo-Particle's ϕ direction combination we minimize a χ^2 function 9.4 via TMinuit, and then perform a weighted sum over all ϕ combinations to create the reconstructed kinematics of the event.

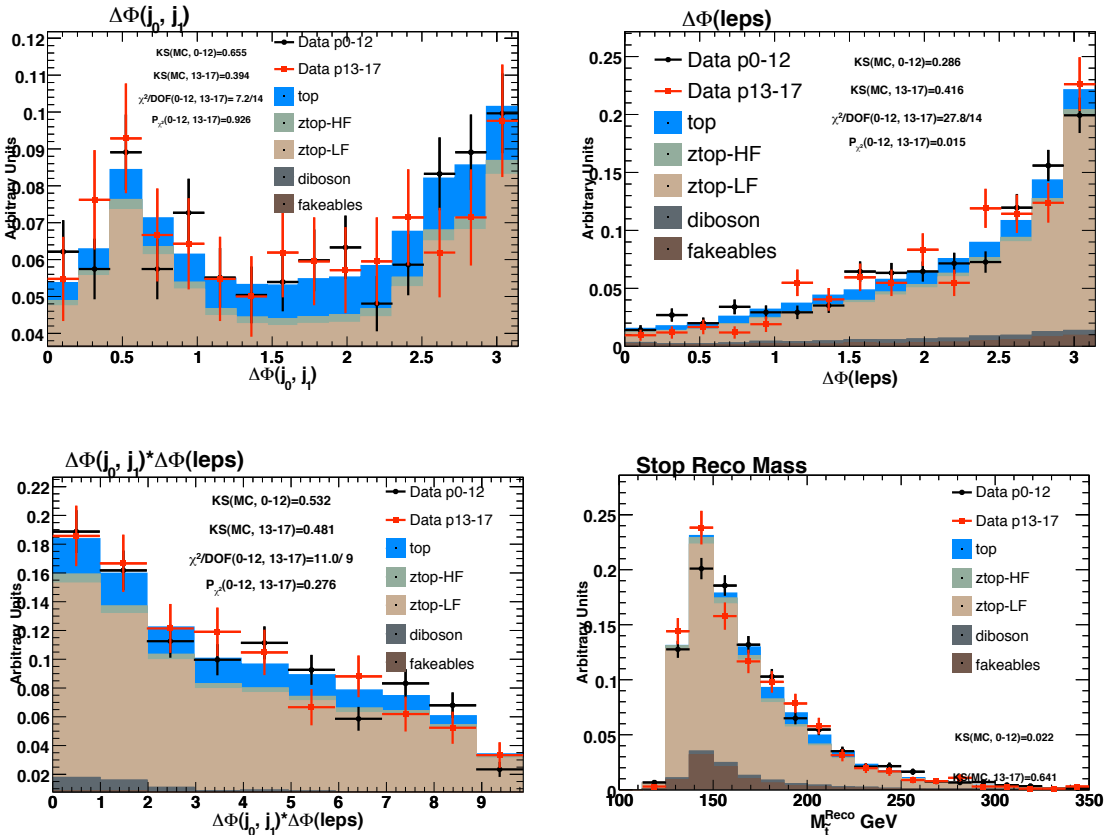

Figure 21: $\Delta\Phi(jet_1, jet_2)$ (upper left), $\Delta\Phi(lep_1, lep_2)$ (upper right), $\Delta\Phi(jet_1, jet_2)$X$\Delta\Phi(lep_1, lep_2)$ (bottom left), and reconstructed stop mass (bottom right), for Opposite-sign events, with $geq2$ jets

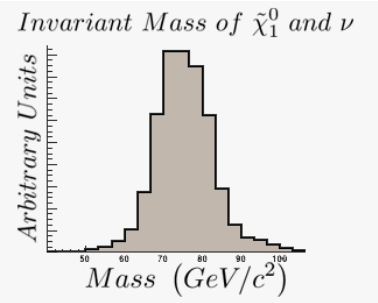

Figure 22: The invariant mass of the Pseudo-Particle ($\tilde{\chi}_1^0 + \nu$) at the generator level, corresponding to $\tilde{t}_1$ mass of 135 GeV, $\tilde{\chi}_1^{\pm}$ mass of 110 GeV, $\tilde{\chi}_1^0$ mass of 60 GeV.

9.4 The χ^2 Minimization Process

We construct the χ^2 function as follows

$$\chi^2 = \frac{\left(\vec{\ell}_{meas} - \vec{\ell}_{fit}\right)^2}{\sigma_\ell^2} + \frac{\left(\vec{\bar{\ell}}_{meas} - \vec{\bar{\ell}}_{fit}\right)^2}{\sigma_\ell^2} + \frac{(\vec{u}_{meas} - \vec{u}_{fit})^2}{\sigma_{uncl}^2}$$
$$+ \sum_{jets\, i} \frac{\left(\vec{j}_{i_{meas}} - \vec{j}_{i_{fit}}\right)}{\sigma_{jet_i}^2} + \frac{\left(M_{PP_1}^{fit} - M_{PP}^{assume}\right)^2}{\Gamma_{PP}^{gen}}$$
$$+ \frac{\left(M_{PP_2}^{fit} - M_{PP}^{assume}\right)^2}{\Gamma_{PP}^{gen}} + \frac{\left(M_{PP_1,\ell} - M_{\tilde{\chi}^\pm}\right)^2}{\Gamma^{\tilde{\chi}^\pm}}$$
$$+ \frac{\left(M_{PP_1,\bar{\ell}} - M_{\tilde{\chi}^\pm}\right)^2}{\Gamma^{\tilde{\chi}^\pm}} + \frac{\left(M_{PP_1,\bar{\ell},b_{jet}} - M_{PP_2,l,\bar{b}_{jet}}\right)}{\Gamma^{\tilde{t}}} \tag{11}$$

where $\vec{\ell}_{meas}$ is the lepton measured momentum and $\vec{\ell}_{fit}$ is the fitted lepton momentum. Similarly u refers to the unclustered energy in the event, which includes all jets except for the assumed b-jets that originate from the stop decay. PP_i are Pseudo-Particles. The first four terms in the χ^2 function refer to how the measured physics quantities are allowed to vary within their estimated uncertainties.

We consider each ϕ-combination of Pseudo-Particles directions, and construct a sum of reconstructed stop masses for all possible combinations that are weighted according to χ^2 of the fit to yield the reconstructed stop mass of an event:

$$M_{\tilde{t}_1}^{Reco} = \frac{1}{\sum_{\phi\, i,j} e^{-\chi_{i,j}^2}} \sum_{\phi\, i,j} M_{i,j}^{fit} e^{-\chi_{i,j}^2} \tag{12}$$

Using the algorithm described above we reconstruct stop masses for our signal and background events. The stop mass distributions are shown in Figure **??**. One can see that the reconstructed mass provides a fairly good discrimination power.

10 Grid Template Morphing

In order to provide a smooth probing of multi-variate SUSY mass space, rather than setting the limits for a few discreet points, we have employed and extended the algorithm to interpolate(morph) templates corresponding to the discreet MC SUSY mass points, we generated. We use an extension of hprizantal morphing, Grid Morphing, which does not ignore the correlations in shape between the different morphing parameters. This allows us to create signal templates anywhere in the SUSY mass space of $m_{\tilde{t}_1}$, $m_{\tilde{\chi}_1^\pm}$, $m_{\chi_1^0}$ that is within the MC points we generated. See [6] for a description of Grid Morphing, and [31] for a good description of horizontal and vertical template morphing techniques.

Events per 2.7 fb^{-1} in the anti-tag signal region

Source	ee	$\mu\mu$	$e\mu$	ll
top	5.9 ± 0.8	5.9 ± 0.9	12.7 ± 1.8	24.5 ± 3.2
ztop-HF	0.4 ± 0.1	0.3 ± 0.1	0.1 ± 0.1	0.7 ± 0.1
ztop-LF	12.5 ± 3.8	8.9 ± 2.7	4.1 ± 0.3	25.5 ± 6.9
diboson	1.9 ± 0.3	1.4 ± 0.3	3.3 ± 0.6	6.5 ± 1.2
fakeables	2.2 ± 0.7	1.8 ± 0.6	5.8 ± 1.8	9.9 ± 3.0
Total	22.8 ± 4.3	18.3 ± 3.3	26.0 ± 4.0	67.2 ± 10.3
stop	1.1 ± 0.5	1.3 ± 0.4	2.9 ± 0.6	5.4 ± 1.5
Data	24	10	25	59

Table 13: Predicted vs observed number of events in the in signal untagged region. Signal monte carlo at $M_{\tilde{t}} = 135, M_{\tilde{\chi}^{\pm}} = 125.8, M_{\tilde{\chi}^{0}} = 58.8\,GeV$ is put in for comparison at br=0.30, the level we exclude at CL=0.95.

Events per 2.7 fb^{-1} in the signal region with ≥ 1 tag.

Source	ee	$\mu\mu$	$e\mu$	ll
top	11.3 ± 1.8	10.4 ± 1.6	26.7 ± 3.8	48.4 ± 7.0
ztop-HF	1.3 ± 0.3	0.9 ± 0.2	0.4 ± 0.1	2.6 ± 0.5
ztop-LF	0.9 ± 0.1	0.5 ± 0.1	0.3 ± 0.1	1.7 ± 0.1
diboson	0.2 ± 0.1	0.1 ± 0.1	0.3 ± 0.1	0.6 ± 0.1
fakeables	0.5 ± 0.2	0.5 ± 0.1	1.8 ± 0.5	2.8 ± 0.8
Total	14.2 ± 2.0	12.4 ± 1.6	29.4 ± 3.8	56.0 ± 7.3
stop	1.1 ± 0.3	1.4 ± 0.4	3.0 ± 0.7	5.5 ± 1.2
Data	15	12	30	57

Table 14: Predicted vs observed number of events in the in signal tagged region. Signal monte carlo at $M_{\tilde{t}} = 135, M_{\tilde{\chi}^{\pm}} = 125.8, M_{\tilde{\chi}^{0}} = 58.8\,GeV$ is put in for comparison at br=0.30, the level we exclude at CL=0.95.

11 Results

The expected numbers of events from various SM backgrounds using event selection cuts as specified in Table 6 are given in Tables 13 and 14 for the anti-tag and the tag region respectively.

In the absence of new physics, we place a limit on the dilepton branching ratio of stop events, at the assumed stop theoretical cross-section

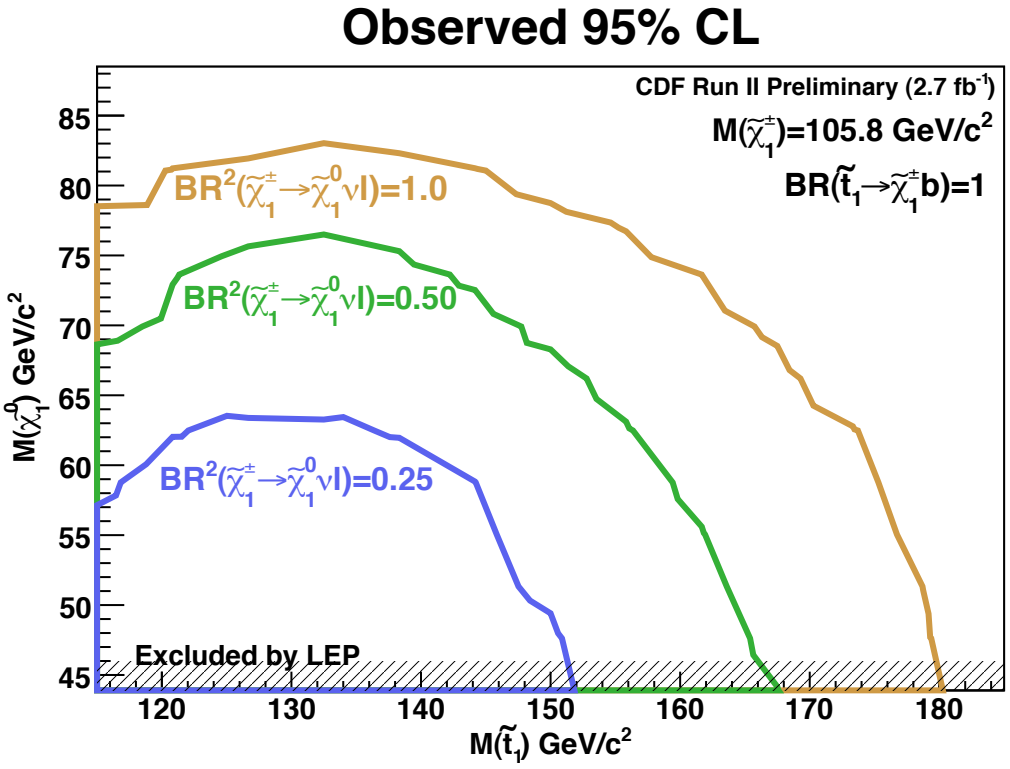

Figure 23: Branching Ratio excluded at th 95% level in the Stop v. Neutralino mass plain, at a chargino mass of 105.8 GeV

References

[1] C. Balazs, M. Carena and C. Wagner, Phys. Rev. **D** 70 (2004) 015007, [arXiv:hep-ph/0403224v2].

[2] W. Beenakker *et al.*, Nucl. Phys. **B**515 (1998) 3-14, [arXiv:hep-ph/9810290].

[3] T. Aaltonen *et al.*, The CDF Collaboration, Phys. Rev. **D**76, 072010 (2007), [arXiv:0707.2567].

[4] W. M. Yao *et al.* [Particle Data Group], J. Phys. G **33**, 1 (2006).

[5] S. Abdullin *et al.*, FERMILAB-CONF-06-284-T, [arXiv:hep-ph/0608322v2].

[6] A. Ivanov *et al.*, CDF Note 9269

[7] T. Affolder *et al.*, The CDF Collaboration, Phys. Rev. Lett. 84, 5273 (2000),(CDF Note 5099)

[8] S.-J. Park, the D0 Collaboration, [arXiv:hep-ph/0710.1016v1].

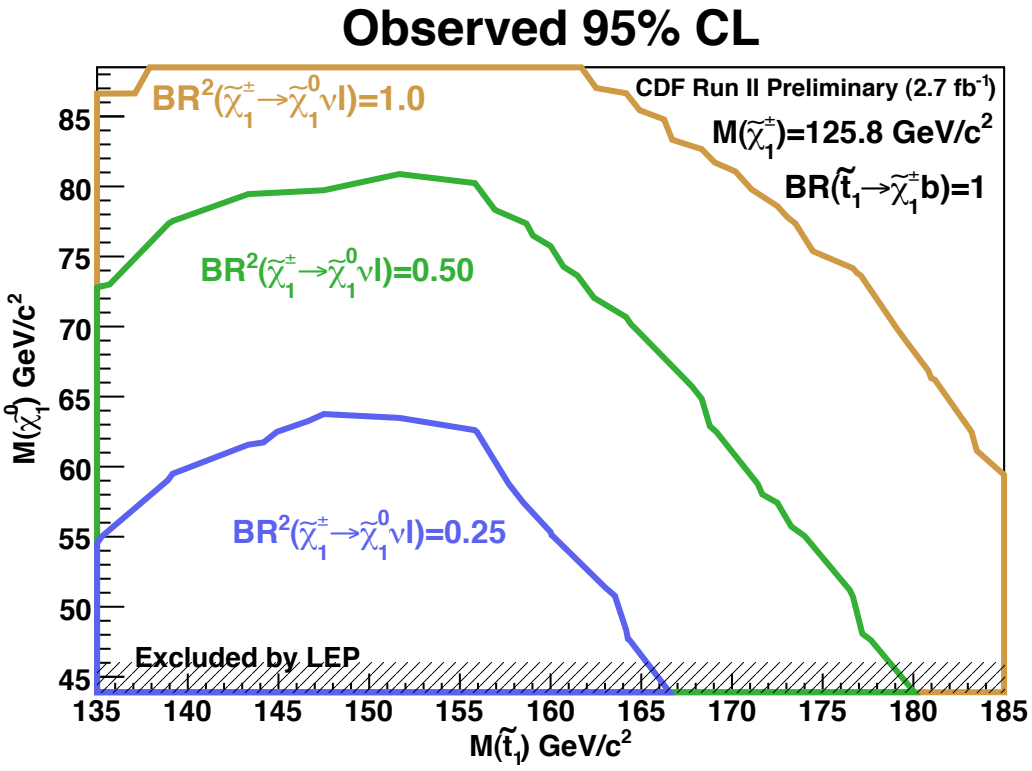

Figure 24: Branching Ratio excluded at th 95% level in the Stop v. Neutralino mass plain, at a chargino mass of 125.8 GeV

[9] W. Yai *et al.*, CDF Note 4394.

[10] B. Jayatilaka *et al.*. CDF Note 9098.

[11] A. Varganov *et al.*, CDF Note 9210.

[12] T. Spreitzer *et al.*, CDF Note 8696.

[13] Top Group Triggers,
http://www-cdf.fnal.gov/tiki/tiki-index.php?page=Checking+Triggers

[14] Top Group Winter 2008 Luminosity, v18,
http://www-cdf.fnal.gov/internal/physics/top/RunIITopProp/gen6Sum06/lumi_v18.html

[15] CDF Good Run List v23
http://www-cdf.fnal.gov/internal/dqm/goodrun/good.html

[16] Baseline High-P_T Electron Selection Criteria,
http://www-cdf.fnal.gov/internal/physics/joint_physics/instructions/electron_cuts_gen6.html

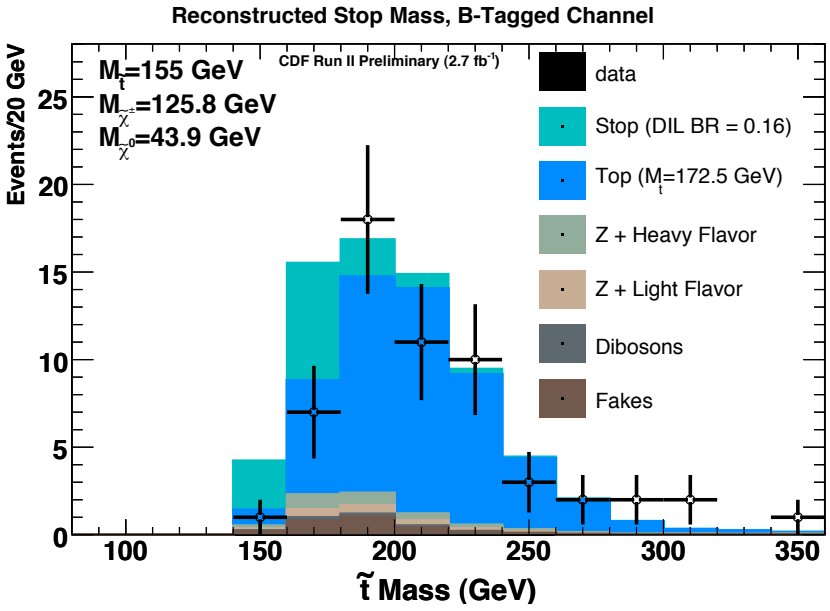

Figure 25: Reconstructed stop mass for $M_{\tilde{t}} = 155, M_{\tilde{\chi}^{\pm}} = 125.8, M_{\tilde{\chi}^0} = 43.9\,GeV$, plotted at the level we exclude at CL=0.95, in the tagged signal region.

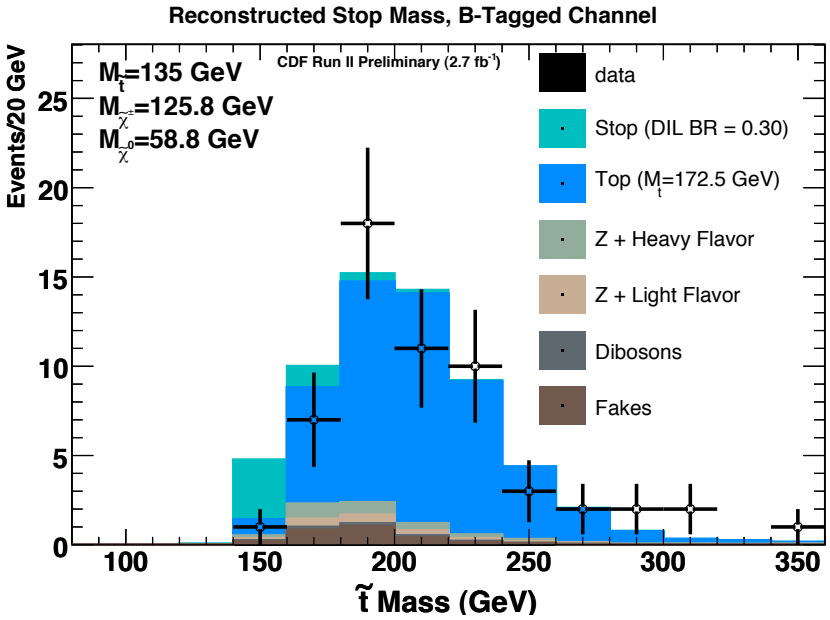

Figure 26: Reconstructed stop mass for $M_{\tilde{t}} = 135, M_{\tilde{\chi}^{\pm}} = 125.8, M_{\tilde{\chi}^0} = 58.8\,GeV$, plotted at the level we exclude at CL=0.95, in the tagged signal region.

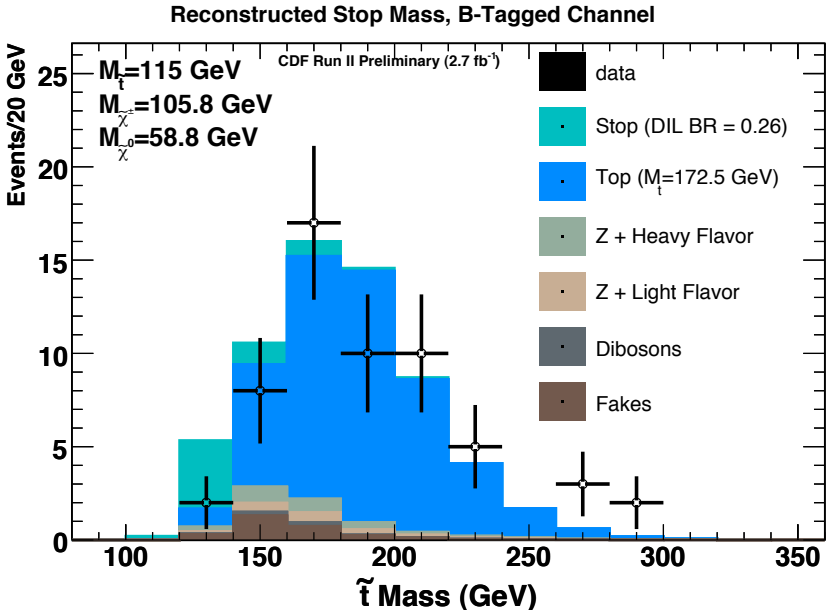

Figure 27: Reconstructed stop mass for $M_{\tilde{t}} = 115, M_{\tilde{\chi}^{\pm}} = 105.8, M_{\tilde{\chi}^0} = 58.8\,GeV$, plotted at the level we exclude at CL=0.95, in the tagged signal region.

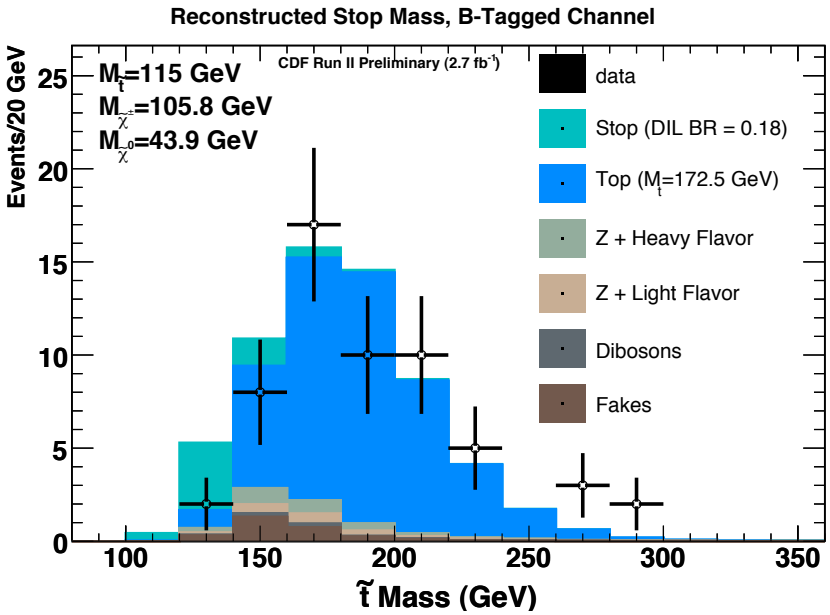

Figure 28: Reconstructed stop mass for $M_{\tilde{t}} = 115, M_{\tilde{\chi}^{\pm}} = 105.8, M_{\tilde{\chi}^0} = 43.9\,GeV$, plotted at the level we exclude at CL=0.95, in the tagged signal region.

[17] Baseline High-P_T Muon Selection Criteria,
http://www-cdf.fnal.gov/internal/physics/joint_physics/instructions/muon_cuts_gen6.html

[18] N. Kimura *et al.*, CDF Note 8904.

[19] CDF lepton trigger efficiencies and scale factors,
http://www-cdf.fnal.gov/internal/physics/joint_physics/instructions/JPScaleFactor

[20] Top Group MC Samples,
http://www-cdf.fnal.gov/internal/physics/top/RunIIMC/topmc6/index.shtml

[21] D. Glenzinski *et al.*, CDF Note 9225.

[22] M. L. Mangano *et al.*, JHEP 0307:001 (2003), [arXiv:hep-ph/0206293].

[23] D. Sherman *et al.*, CDF Note 8767.

[24] C. Plager*et al.*, CDF Note 9161.

[25] S. Grinstein and D. Sherman, CDF Note 8910.

[26] I. Zaw, Method II workshop, May 11, 2007,
http://www-cdf.fnal.gov/internal/WebTalks/Archive/0705/070511_method_2_workshop

[27] CDF Technical Design Report, FERMILAB-Pub-96/390-E.

[28] Jet Energy and Resolution Group,
http://www-cdf.fnal.gov/internal/physics/top/jets/corrections.html

[29] A. L. Read, Nucl. Instrum. Meth. **A425** (1999), 357-360.

[30] T. Junk, CDF Note 8128.

[31] T. Junk, Talk at the CDF Top Meeting, June 28, 2007
http://www-cdf.fnal.gov/internal/WebTalks/Archive/0706/070628_top/

[32] **TMVA** ,Toolkit for Multivariate Analysis with Root,
http://tmva.sourceforge.net/

[33] M. Cacciari *et al.*, JHEP **0404** (2004) 068, [arXiv:hep-ph/0303085v1].

[34] E. Brubaker *et al.*, CDF Note 6845.

[35] J. Konigsberg *et al.*, CDF Note 7446.

[36] S. M. Wang *et al.*. CDF Note 8290